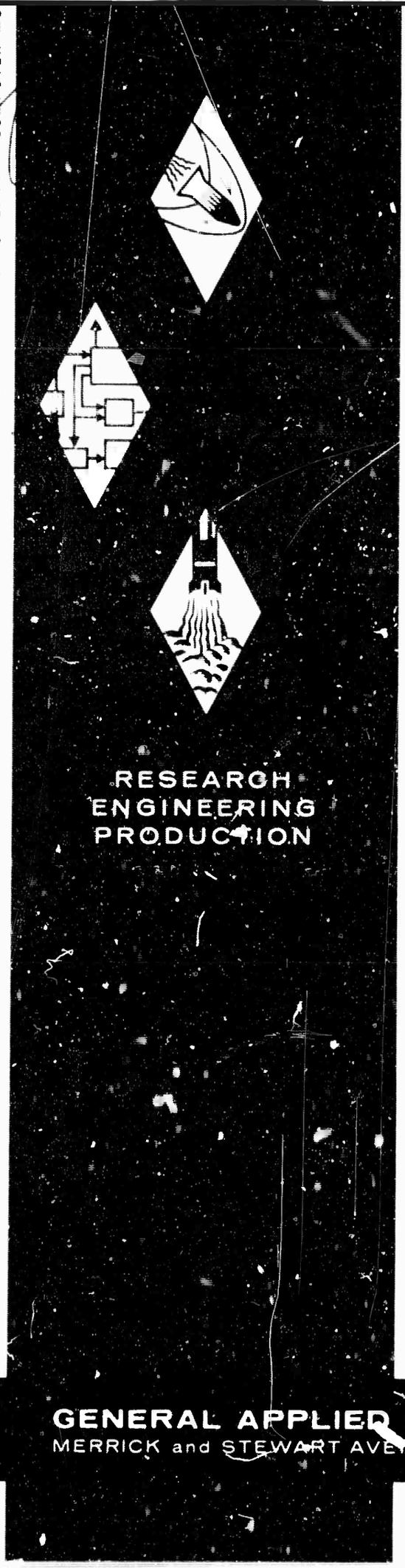

AEROSPACE RESEARCH • AERODYNAMICS • PROPULSION • STRUCTURAL DYNAMICS • ELECTRONIC SYSTEMS AND INSTRUMENTS • COMPUTER MO

HEAT TRANSFER DUE TO COMBUSTION ON A FLAT PLATE IN SUPERSONIC FLOW

GASL TECHNICAL REPORT NO. 486

by: W. Chinitz & L. Spadaccini

GENERAL APPLIED SCIENCE LABORATORIES, INC.
MERRICK and STEWART AVENUES, WESTBURY, L.I., N.Y. (516) ED 3-6960

HEAT TRANSFER DUE TO COMBUSTION ON A FLAT PLATE IN SUPERSONIC FLOW

GASL TECHNICAL REPORT NUMBER 486

by: W. Chinitz and L. Spadaccini

A PROJECT DEFENDER RESEARCH STUDY

Sponsored by the

Advanced Research Projects Agency
(Ballistic Missile Defense Engineering Office)
Washington 25, D.C.

ARPA ORDER NUMBER 460

Prepared by

General Applied Science Laboratories, Inc.
Merrick and Stewart Aves.
Westbury, L.I., New York

December 1964

Approved by: _____
Antonio Ferri
President

FOREWORD

This research was supported by the Advanced Research Projects Agency (Ballistic Missile Defense Engineering Office) as part of Project DEFENDER, under the technical direction of Mr. V. S. Kupelian, and was monitored by the U.S. Army Missile Command under Contract Number DA-30-069-AMC-216(Z).

SUMMARY

A theoretical and experimental investigation was undertaken of heat transfer effects at the surface of a flat plate on which combustion is occurring in a supersonic air stream. A simplified theoretical model is developed which leads to expressions for the heat transfer coefficient and heat transfer rate at the surface. The experimental technique used to obtain heat transfer parameters is described. The experimental tests were conducted at Mach number 3.1 using the pyrophoric fuel triethylaluminum. A comparison between the theoretical and experimental results indicates that the former yields order-of-magnitude estimates of the heat transfer coefficient and rate which are satisfactory for purposes of engineering design. The theory is then used to obtain estimates of heat transfer parameters at the surface of a cone-shaped interceptor executing a coast trajectory. The results are shown to be well correlated by an empirical expression similar to that encountered in the literature for turbulent non-reacting flow over flat plates having both constant and variable surface temperatures.

TABLE OF CONTENTS

LIST OF FIGURES

LIST OF FIGURES (contd)

LIST OF SYMBOLS

a	velocity of sound
B	semi-empirical Blasius parameter
b	semi-empirical Blasius parameter
C_f	skin friction coefficient
Ch	dimensionless chemical energy grouping, Eq. (21)
c_p	specific heat at constant pressure
f	stoichiometric fuel-air ratio by weight
H_c	heat of combustion
h_c	chemical enthalpy
h_s	total sensible enthalpy
h	heat transfer coefficient at surface
k	thermal conductivity of combustion gas
L	characteristic length of the system
M	Mach number, u/a
$\mathcal{m}$	molecular weight
$\dot{m}_f$	mass flow rate of fuel
Nu	Nusselt number, hL/k
Pr	Prandtl number, $c_p \mu/k$
p	pressure
q	heat flux into control volume
q_c	chemical energy flux per unit length
q_w	heat flux per unit area to surface
R_o	universal gas constant
Re_x	Reynolds number based on plate length, $\rho x u/\mu$
Re_Γ	Reynolds number based on stagnation temperature thickness, $\rho \Gamma U_\infty/\mu$
R	recovery factor, Eq. (13)
St	Stanton number, $h/\rho c_p u$
T	static temperature
T_o	stagnation temperature
U_∞	flame zone velocity

LIST OF SYMBOLS (contd)

u	velocity
x	coordinate parallel to free-stream velocity vector
y	coordinate normal to plate surface
z	coordinate in the plane of the plate and normal to x
β	defined by Eq. (28)
Γ	stagnation temperature thickness, Eq. (6)
γ	ratio of specific heats
δ	boundary layer thickness
η	equivalence ratio (fuel-air ratio/fuel-air ratio at stoichiometric)
μ	viscosity
ρ	density
ω	viscosity-temperature exponent, Eq. (25)

Subscripts and Superscripts

a	air
ad	adiabatic conditions
f	fuel
i	free-stream conditions
w	conditions at surface
∞	flame zone conditions
1,2,3	refers to fluid entering or leaving control volume
*	refers to empirical reference state

I. INTRODUCTION

A number of schemes exist for utilizing a combustion process to produce aerodynamic lift forces[1,2], vehicle control forces[3-8], and thrust vector control of rocket motors[9-11]. In each case, the underlying principle is the same: To inject and burn a combustible liquid or gas at some surface in a supersonic flow environment, leading to a deflection of streamlines and attendant pressure increases.

One of the problems introduced by the application of combustion at a surface is the need for a priori estimates of the surface heat transfer to ensure an appropriate design. In the following section, an approximate theoretical analysis is developed for calculating the heat transfer to a turbulent flat plate in the presence of heat generated by combustion. In an effort to determine the effectiveness of this analysis in predicting heat transfer rates and coefficients, a series of experiments was undertaken in which the pyrophoric fuel triethylaluminum (TEA) was injected and burned at the surface of a flat plate in Mach 3.1 flow. The details of these experiments are contained in Reference 4, and are briefly summarized in Section III.A of this report.

During these tests, the plate surface temperature was monitored by a heat transfer gage of special design, which is described in Section III.A. From these readings, heat transfer coefficients and heat transfer rates at the plate surface were deduced (Section III.B). The experimental results obtained by this means are presented in Section III.C.

The theoretical and experimental results are compared in Section IV. As an example of the use of the theoretical analysis

in obtaining estimates of heat transfer coefficients and heat transfer rates, these parameters are calculated for the case of external burning employed to generate a control force on a cone-shaped interceptor executing a coast trajectory (Section V). Throughout these calculations, the fuel considered is TEA; however, this fuel is sufficiently similar to most hydrocarbon fuels ($H_c \approx 18{,}000$ BTU/lbm) to permit the use of these results in estimating heat transfer coefficients and rates on vehicles executing similar maneuvers and using other hydrocarbon-like fuels.

II. THEORETICAL HEAT TRANSFER ANALYSIS

An approximate model of heat transfer to a flat plate in the presence of combustion may be formulated by a modification of the analysis developed by Mayer[12]. The two-dimensional model employed is depicted in Figure 1. Here, conditions denoted by the subscript ∞ refer to conditions in the flame zone where the stagnation temperature is varying with x, rather than the inviscid nozzle flow field examined by Mayer. Effects such as the deposition of insulating solids on the surface and radiation are neglected.

Referring to Figure 1b, the various energy terms entering the control volume are understood to include both sensible and chemical energies. Thus,

$$dq_1 = dh_{s,1} + dh_{c,1} = \int_0^\delta \rho u c_p T_o \, dy + dh_{c,1} \tag{1}$$

where h_s is the total sensible enthalpy (including kinetic energy) and h_c is the chemical enthalpy. In like manner,

$$dq_2 = c_p T_{o,\infty} \frac{d}{dx} \left[\int_0^\delta \rho u dy \right] dx + dh_{c,2} \tag{2}$$

$$dq_3 = \int_0^\delta \rho u c_p T_o dy + \frac{d}{dx} \left[\int_0^\delta \rho u c_p T_o dy \right] dx + dh_{c,3} \tag{3}$$

Application of the conservation of energy to the control volume leads to

$$q_w = c_p T_{o,\infty} \frac{d}{dx} \int_0^\delta \rho u \left[1 - \frac{T_o}{T_{o,\infty}} \right] dy + \frac{dq_c}{dx} \tag{4}$$

where dq_c represents the net amount of energy entering the control volume by virtue of the addition of chemical energy. At the edge of the boundary layer, the gas dynamic conditions approach conditions in the flame zone. If it is assumed that the flame zone extends well above the plate surface, and that conditions in this region are independent of y, Equation (4) may be written to a fair degree of approximation:

$$q_w = c_p T_{o,\infty} \frac{d}{dx} \int_o^\infty \rho u \left[1 - \frac{T_o}{T_{o,\infty}}\right] dy + \frac{dq_c}{dx} \qquad (5)$$

A "stagnation temperature thickness" is introduced defined by

$$\Gamma \equiv \frac{1}{\rho_\infty U_\infty} \int_o^\infty \rho u \left[1 - \frac{T_o}{T_{o,\infty}}\right] dy \qquad (6)$$

which has dimensions of length. The thermal Reynolds number is then defined as

$$Re_\Gamma \equiv \frac{\rho_\infty U_\infty \Gamma}{\mu_\infty} \qquad (7)$$

Introducing these terms into Equation (5), and initially assuming that c_p, μ, and Pr are constants at flame zone conditions (the case of variable μ, and c_p and Pr taking on constant values other than ∞ will be treated subsequently), leads to

$$q_w = \mu_\infty c_{p_\infty} T_{o,\infty} \frac{d}{dx} Re_\Gamma + \frac{dq_c}{dx} \qquad (8)$$

Introducing the adiabatic heat transfer coefficient and Starton number, respectively:

$$h \equiv \frac{q_w}{T_{ad}-T_w} \tag{9}$$

$$St \equiv \frac{h}{\rho_\infty c_{p_\infty} U_\infty} \tag{10}$$

Equation (8) becomes

$$\frac{d}{dx} Re_\Gamma = \frac{\rho_\infty U_\infty}{\mu_\infty} \left[\frac{T_{ad}-T_w}{T_{o,\infty}}\right] St - q_c^* \tag{11}$$

in which

$$q_c^* = \frac{1}{\mu_\infty c_{p_\infty} T_{o,\infty}} \cdot \frac{dq_c}{dx} \tag{12}$$

A semi-empirical recovery factor is now employed, defined as

$$R \equiv \frac{T_{ad} - T_\infty}{T_{o,\infty} - T_\infty} \tag{13}$$

where $R = Pr^{1/3}$ for turbulent boundary layers[12]. Using the relation

$$T_{o,\infty} = T_\infty \left[1 + \frac{\gamma-1}{2} M_\infty^2\right] \tag{14}$$

in Equation (13) leads to the following expression for the adiabatic wall temperature:

$$T_{ad} = T_{o,\infty} \left[\frac{R\left(\frac{\gamma-1}{2} M_\infty^2\right)+1}{1+\frac{\gamma-1}{2} M_\infty^2}\right] \tag{15}$$

Following Mayer, we now assume that the relation between Re and St, which is necessary to solve Equation (11), is the same relation which may be derived for the case of uniform flow along

a flat plate. This latter expression may be obtained as follows:

The Blasius equation for the skin friction on a flat plate for constant fluid properties is

$$\frac{C_{f,\infty}}{2} = B\, Re_{x,\infty}^{-b} \tag{16}$$

A modified Reynolds analogy is employed:

$$St_{\infty} = \frac{C_{f,\infty}}{2} Pr_{\infty}^{-2/3} = B\, Pr_{\infty}^{-2/3}\, Re_{x,\infty}^{-b} \tag{17}$$

where the semi-empirical Blasius parameters have the values $b = 1/5$, $B = 0.0296$ for a turbulent flat plate boundary layer, and the Reynolds number is given by $Re_{x,\infty} = \rho_{\infty} U_{\infty} x/\mu_{\infty}$.

Substitution of Equation (17) into Equation (11) gives

$$\frac{d}{dx} Re_{\Gamma} = \frac{\rho_{\infty} U_{\infty}}{\mu_{\infty}} \left(\frac{T_{ad}-T_w}{T_{o,\infty}} \right) BPr^{-2/3}\, Re_{x,\infty}^{-b} - q_c^* \tag{18}$$

In order to integrate Equation (18), the following simplifying assumptions will be made:

1. The term $(T_{ad}-T_w)/T_{o,\infty}$ will be assumed to be independent of x. This assumption was employed by Mayer as well as for flow through a rocket nozzle, and an a posteriori examination of the results generated by this analysis indicates that this parameter changes by only 4 or 5% in going from $(x/L)=0$ to $(x/L)=1$, where L is the plate length.

2. In integrating the second term in Equation (18), $T_{o,\infty}$ will be assumed independent of x. The justification for this assumption is that a comparison between the analytical and experimental results (Section IV) indicates that the local equivalence ratio (fuel-air ratio/fuel-air ratio at stoichiometric)

in the vicinity of the plate is substantially less then unity, resulting in relatively small increases in $T_{o,\infty}$ as x increases. This also has the advantage of delaying the necessity for specifying $q_c(x)$, thereby generalizing the final result.

Employing these two assumptions, integration of Equation (18) yields

$$Re_\Gamma = \left(\frac{T_{ad}-T_w}{T_{o,\infty}}\right) \frac{B\ Pr_\infty^{-2/3}\ Re_{x,\infty}^{(1-b)}}{1-b} - \frac{q_c}{\mu_\infty c_{p_\infty} T_{o,\infty}} \qquad (19)$$

where the initial conditions that Re_Γ and q_c are zero at x=0 were used.

Using Equation (17) in Equation (19) leads to

$$Re_\Gamma + Ch = \frac{(BPr_\infty^{-2/3})^{1/b}}{1-b} \left(\frac{T_{ad}-T_w}{T_{,\infty}}\right) (St_\infty)^{\frac{(1-b)}{-b}} \qquad (20)$$

in which the dimensionless "chemical energy number" is given by

$$Ch \equiv \frac{q_c}{\mu_\infty c_{p_\infty} T_{o,\infty}} \qquad (21)$$

Equation (20) may now be used in Equation (11) to obtain the following first-order differential equation:

$$\frac{1}{St}\frac{d}{dx}(St)^{\frac{(1-b)}{-b}} = \frac{\rho_\infty U_\infty}{\mu_\infty} \cdot \frac{(1-b)}{(B\ Pr_\infty^{-2/3})^{1/b}} \qquad (22)$$

which, upon integration and using Equation (10), leads to

$$h = \frac{B\ Pr_\infty^{-2/3}\ \rho_\infty\ c_{p_\infty} U_\infty}{Re_{x,\infty}^{b}} \qquad (23)$$

The initial condition $St \longrightarrow \infty (Re_T=0)$ at x=0 was employed above.

The effect of variable density and viscosity may now be introduced in the following manner:

We assume that all fluids are ideal gases, so that

$$\rho \propto T^{-1} \tag{24}$$

and that the viscosity is a function of temperature only; this functional relationship may be written

$$\mu \propto T^{\omega} \tag{25}$$

where ω is an empirically-determined parameter. The Prandtl number and specific heat are assumed to be constant at some mean value between $T_{o,\infty}$ and T_w (i.e., $\bar{Pr}=Pr, c_p=\bar{c}_p$).

We now employ Eckert's reference temperature method as suggested by Mayer[12], in which the modified Stanton number (to account for the variable fluid properties) may be written

$$\frac{St}{St_\infty} = \left(\frac{\mu_\infty}{\mu^*}\right)^{-b} \left(\frac{\rho^*}{\rho_\infty}\right)^{1-b} \tag{26}$$

where μ^* and ρ^* are evaluated at an empirical reference temperature given by

$$T^* = \tfrac{1}{2}(T_w+T_\infty) + 0.22\,(T_{ad}-T_\infty) \tag{27}$$

Using Equations (24) and (25) in Equation (26) yields

$$\frac{St}{St_\infty} = \left(\frac{T_\infty}{T^*}\right)^{1-b(1+\omega)} \equiv \beta \tag{28}$$

Therefore, Equation (17) and (28) lead to

$$St = \beta\, St_{\infty} = \frac{\beta\, B \overline{Pr}_{\infty}^{-2/3}}{Re_{x,\infty}^{b}} \tag{29}$$

Substituting Equation (29) into Equation (11) and integrating the resulting expression gives

$$Re_{\Gamma} + Ch = \left(\frac{T_{ad}-T_{w}}{T_{o,\infty}}\right) \frac{(\beta\, B\, \overline{Pr}_{\infty}^{-2/3})^{1/b}}{1-b}\, St^{\frac{(1-b)}{-b}} \tag{30}$$

where Equation (17) was also used. Once again, the initial condition $Re_{\Gamma} = Ch = 0$ at $x=0$ was employed.

Resubstituting this result back in Equation (11) gives the following first-order differential equation:

$$\frac{1}{St} \cdot \frac{d}{dx} \beta^{1/b}\, St^{\frac{(1-b)}{-b}} = \frac{1-b}{(B\, \overline{Pr}^{-2/3})^{1/b}} \cdot \frac{\rho_{\infty} U_{\infty}}{\mu_{\infty}} \tag{31}$$

which may be integrated (employing a substitution of variables, $G=\beta^{\frac{1}{1-b}} St$) to give

$$h = \frac{\beta^{\frac{1}{1-b}} (B\, \overline{Pr}^{-2/3}) (\rho_{\infty} \overline{c}_{p} U_{\infty})}{\left[\int_{o}^{x} \beta^{\frac{1}{1-b}} \rho_{\infty} U_{\infty} \mu_{\infty}^{-1}\, dx\right]^{b}} \tag{32}$$

where Equation (10) and the initial condition $St \longrightarrow \infty$ at $x=0$ were used.

It is of interest to note that Equations (23) and (32) are identical in form to the equivalent expressions derived by Mayer. This stems from the two major assumptions mentioned above which permitted the lumping of the thermal Reynolds number, Re_Γ, and the chemical energy number, Ch, into an effective single dimensionless grouping, $(Re_\Gamma + Ch)$. For the case of a flat plate, and substituting the empirically-determined values of b and B, Equation (32) becomes

$$h = \frac{0.0296\ \beta\ \bar{Pr}^{-2/3}}{Re_{x,\infty}^{1/5}} \frac{\rho_\infty\ \bar{c}_p\ U_\infty}{} \qquad (33)$$

and the heat transfer rate to the wall may be obtained from Equation (9). It remains to specify some suitable relation for $T_{o,\infty}(x)$, which may, of course, be empirically-determined, and to choose the viscosity relationship, Equation (25).

For simplicity, we assume a relationship between the chemical heat input and the flame zone stagnation temperature of the form

$$xq_c = \dot{m}_f\ \bar{c}_p\ (T_{o,\infty} - T_{o,i}) \qquad (34)$$

which may be manipulated to yield

$$T_{o,\infty} = \frac{\eta f H_c}{\bar{c}_p} \left(\frac{x}{L}\right) + T_{o,i} \qquad (35)$$

where η is the equivalence ratio, f is the stoichiometric fuel-air ratio, and H_c is the heat of combustion of the fuel.

A reasonable empirical expression for the viscosity-temperature relationship is

$$\mu_{\infty} = 0.835 \times 10^{-7} \cdot T^{0.76} \text{ lbm/ft-sec} \qquad (36)$$

which is shown in Figure 2 along with viscosities of the species likely to be found in large quantities in the flame zone. It may be seen that Equation (36) provides a suitable average flame zone viscosity over a wide range of temperature.

It should be noted that in the above analysis thermochemical and kinetic effects, of the type examined by Rosner[13] have not been included. It will be seen (Section IV) that the simplified model presented above yields results which are in reasonably good quantitative agreement with experimental results, and, as a consequence, supplies estimates of the heat transfer coefficient and heat transfer rate which are sufficiently accurate for most engineering purposes.

It will be shown in Section IV that for given flame zone conditions, neither the equivalence ratio, molecular weight, nor Prandtl number substantially affect the value of heat transfer coefficient, and that only η affects the heat transfer rate to the wall to a substantial extent. This latter effect stems from the direct relationship between T_{ad} and η through Equations (15) and (35). The insensitivity of h to the parameters mentioned above permits a wide latitude in the estimation of these parameters and circumvents the need for an extensive chemical equilibrium analysis of the combustion process to determine accurate values for $\mathcal{M}$ and $\overline{Pr}$.

III. EXPERIMENTAL TECHNIQUES

A. Description of Experimental Apparatus

The experimental program was conducted in the GASL Mach number 3.1 high-temperature blowdown wind tunnel using the pyrophoric fuel triethylaluminum (TEA). The nominal operating conditions were 100-250 psia stagnation pressure and 1500-2500°R stagnation temperature. The tunnel is described in greater detail in Reference 4. TEA was injected through an axially-aligned, triangular-shaped pattern of injector holes shown with the model in Figure 3.

Since the stagnation conditions were not invariant with time, a transient heat transfer measuring technique was employed. The conventional thin-walled model technique which is frequently used in connection with transient heat transfer experiments is not applicable here because of wind tunnel limitations. The time for the tunnel to achieve steady flow is approximately five seconds; therefore, it is impossible to obtain a temperature history which reflects only the steady-flow conditions. Thus, for the heating rates available the model must be thick and not thin. It was therefore decided to use the method discussed by Cresci and Libby[14]. This technique is also a transient one and involves a cylindrical plug attached to the model at the surface but insulated from it for the remaining portion of its length by an air gap (Figure 4). It is assumed that this gap acts as a sufficiently good insulator to prevent any heat transfer between the plug and the surrounding body, thus permitting heat flow only parallel to the plug axis. This arrangement transforms the unsteady heat

conduction problem from one involving axial and radial conduction into one which is locally only one-dimensional and analogous to a rod heated at one end. In general, if the surface temperature history and the initial temperature distribution in the plug are known, the solution for the rate of heat transfer to the plug can be determined. The initial temperature distribution in the plug is assumed to be constant and care is taken to establish such a state prior to testing. The surface temperature history is determined by a thermocouple located at the plug surface.

The junction of the thermocouple is made as close to the surface as possible by the following technique: The individual thermocouple wire insulation is drawn up through a small hole in the plug at the surface, then a tapered pin of the same material as the model and plug is driven into the hole so as to cut the insulation against the wall of the plug at the surface. The pin is filed off and the surface smoothed. The thermocouples are then checked to detect buried junctions by applying a small heat input and observing the response time.

B. Heat Transfer Gage Analysis

For relatively low rates of heat transfer or short periods of heating, the thermocouple plug can be considered a semi-infinite solid. That is, the inside surface of the plug is assumed to remain at essentially the same temperature as it was at the initiation of heating. To obtain a general solution to the heat conduction equation, temperature at the surface is considered an arbitrary function of time. This method gives local values at each interval of time and eliminates the effect of non-uniform starting conditions.

For the following boundary conditions:

$T = T_i$ at $t=0$

$T = T_i + \varphi(t)$ at $y=0$

$T = T_i$ at $y=\infty$

it can be shown[14] that by integrating the partial time derivative of the temperature from zero to infinity, the heat transfer is:

$$q_{x=0} = \sqrt{\frac{\rho c k}{\pi}} \int_0^t \varphi'(\lambda)\ (t-\lambda)^{-1/2}\ d\lambda \qquad (37)$$

For numerical integration and data reduction, Equation (37) can be approximated by

$$q_{x=0} \sqrt{\frac{\rho c k}{\pi}} \left[2\sqrt{\epsilon}\ \varphi'(t) + \frac{\varphi(t-\epsilon)}{\epsilon^{1/2}} - \int_0^{t-\epsilon} \frac{\varphi(\lambda)}{2(t-\lambda)^{3/2}} \right] d\lambda \qquad (38)$$

where $\epsilon > 0$ and is selected such that

$$\varphi'(\lambda) \cong \varphi'(t) \quad \text{for} \quad t-\epsilon \leq \lambda \leq t$$

Thus, for any measured surface temperature history, the aerodynamic heat transfer rate can be determined from Equation (38).

C. Experimental Results

Tests were conducted at Mach number 3.1 and nominal stagnation pressures of 110 and 250 psia. The basic data were: heat transfer coefficient, heat transfer rate, surface temperature distribution, stagnation temperature, and injectant mass flow rate. The variation of these parameters with time is presented in Figures 5 and 6.

It is observed in Figure 5 that for tests conducted at 110 psia stagnation pressure (p_i=2.63 psia) and stagnation temperature approximately 2300°R, the centerline heat transfer coefficient and heat transfer rate 2.5 inches downstream of the injector stabilize at some value and then decrease with increased injectant mass flow. This point is significant since it appears that for given stagnation conditions there exists an optimum injectant mass flow rate which if exceeded results in a decrease in $h(x)$ and $q_w(x)$. A similar existence of an optimum mass flow was noted earlier in the force production mechanism, described in Reference 3, and was attributed to cooling of the combustion gases by unburned fuel. This cooling coupled with the corresponding local pressure decrease due to droplet breakup, evaporation effects and local aerodynamic expansions tend to lower the efficiency of the combustion process and result in a corresponding decrease in $h(x)$ and $q_w(x)$, shown as functions of injectant mass flow in Figure 7a.

Tests at 200 psia stagnation pressure (p_i=4.7 psia) and 1500-1900°R stagnation temperature resulted in opposite trends in the heat transfer rate and heat transfer coefficient data 6.5 inches downstream of the injector (Figure 6 and 7b). This result, which was partially due to decreasing stagnation temperature, demonstrates the greater dependence of $q_w(x)$ on ignition delay and chemical reaction times. This effect is explained in detail in Section IV.

The development of the combustion process along the surface of the model may be traced by reference to the axial gradient of $h(x)$ and $q_w(x)$ (Figure 8). For the low pressure case this gradient initially decreases, indicating a constant

or decreasing effective local equivalence ratio, and then increases downstream as the fuel spreads on the surface of the model and more air becomes available. In the high pressure case the gradient continuously increases, indicating a steadily-increasing local equivalence ratio.

Finally, in Figure 9 it is shown that the reaction is approximately symmetric about the centerline and also that a more efficient burning process occurs as one proceeds from the centerline toward the outer edge of the flat plate model, (in the direction of increasing z). This latter phenomenon implies that a fuel-rich condition most likely exists along the plate centerline, which becomes more nearly stoichiometric in proceeding to the outer boundary of the flame zone.

IV. COMPARISON BETWEEN THEORY AND EXPERIMENT

In order to determine the effectiveness of the theoretical analysis (detailed in Section II) in predicting heat transfer coefficients and rates, a comparison for two typical experimental runs is made in this section. The test conditions chosen for comparison are tabulated in Figure 10-13. The times were chosen as being representative of periods when a quasi-steady-state was achieved. (Section III, Figures 5 and 6).

Comparison between the theoretical and experimental values of $h(x)$ and $q_w(x)$ for the two typical runs are shown in Figures 10 through 13. It may be seen that, in spite of the limitations imposed by the assumptions used in the analysis of Section II, both $h(x)$ and $q_w(x)$ agree with the experimental values to within an order-of-magnitude when a fixed value of $\eta = 0.01$ is used, in spite of the fact that the experimental flame was not two-dimensional[4]. It will be seen presently that the theoretical value of $h(x)$ is fairly insensitive to η. However, $q_w(x)$ depends upon η to a much larger extent. When a low value of η is chosen $\eta = 0.01$, the $q_w(x)$ values (Figures 11 and 13) are in reasonably good quantitative agreement. The corresponding values of $h(x)$ for this value of η are shown in Figures 10 and 12.

The differences in the sign of the slopes of the theoretical and experimental curves most likely stems from a variation in the value of the equivalence ratio with plate length in the experimental case. That is, there is experimental evidence[3,4] which indicates that the overall chemical reaction accelerates as x increases, because of droplet breakup, evaporation effects, and changes in the ignition delay and chemical reaction times resulting from variations in the local environmental conditions. The variable η curve in Figure 13, in which a linear increase of

η with x was arbitrarily taken, demonstrates that theoretical curves with slopes having the same sign as the experimental curves can be generated by including in the calculation this additional experimentally-observed effect. However, the order-of-magnitude agreement obtained with constant η is regarded as sufficiently accurate to provide satisfactory engineering estimates of heat transfer coefficients and rates.

In obtaining the theoretical estimates of $h(x)$ and $q_w(x)$ shown in Figures 10 through 13, the following values of input parameters, characteristic of TEA combustion and the experimental conditions, were emp'oyed:

$$f_{TEA} = 0.08 \text{ lbm}_f/\text{lbm}_a$$

$$H_{c,TEA} = 18,300 \text{ BTU/lbm}_f$$

$$\overline{Pr} = 0.75$$

$$\overline{c}_p = 0.30 \text{ BTU/lbm-}^{\circ}\text{R}$$

$$\mathcal{M} = 28 \text{ lbm/lb-mole}$$

$$\eta = 0.01$$

$$T_{o,i} = 2300^{\circ}\text{R}$$

$$p_{\infty} = 4.2 \text{ psia}$$

$$M_{\infty} = 1.25$$

$$L = 10.25 \text{ in.}$$

The chosen value of p_∞ represents the average of the values at the plate surface as measured by a large number of static pressure taps. The value of M_∞ was chosen as follows:

In these experiments, the combustion process forms an approximate half-cone region which tends to divert the streamlines in much the same way as a solid half-cone[4]. By measuring the cone angle from photographs and using cone charts[14], the approximate Mach number at the edge of the burning zone can be calculated. Billig[5] shows that the variation of Mach number from the wall through the combustion region is approximately linear. As a result, an average Mach number in this zone may be taken as one-half the value at the outer edge of the burning region.

Clearly, further manipulation of such parameters as η, p_∞ and M_∞ can bring the theoretical and experimental values of $h(x)$ and $q_w(x)$ still closer. However, for present purposes, such empirical manipulation is not deemed warranted.

It is instructive to examine the effect of certain parameters on the values of h and q_w. Figure 14 shows the effect of varying the equivalence ratio, η. As was previously mentioned, changing η by a factor of ten results in a relatively small change in h; however, the wall heat transfer varies substantially. As pointed out in Section II, this latter effect stems from the dependence of T_{ad} on η through Equations (15) and (35).

The effect of a specific heat variation is shown in Figure 15. As may be seen, a 20% variation in $\bar{c}_p$ leads to a corresponding change in h and q_w, primarily through the direct dependence on h on $\bar{c}_p$ in Equation (33). However, the flame zone specific heat for hydrocarbon-like fuels changes relatively little over wide

ranges of pressure, temperature and equivalence ratio[15]. As a result, this parameter can be estimated with reasonable accuracy from existing data.

The effects of molecular weight and Prandtl number changes are shown in Figures 16 and 17. In both cases, h and q_w change very little, indicating that highly accurate estimates of these parameters are not required for present purposes.

The fairly wide margin of uncertainty which can be tolerated in the estimation of input parameters, adds to the utility of the theoretical analysis in estimating heat transfer coefficients and rates encountered on the surface of a flight vehicle on which combustion is occurring. Such estimates are discussed in the next section.

V. THEORETICAL HEAT TRANSFER RESULTS CORRESPONDING TO FLIGHT CONDITIONS

The mission selected for evaluation involves the uniformly-decelerating coast trajectory executed by an 8° half-angle cone from 10,000 fps at 3000 foot altitude to 6000 fps at 20,000 feet. The burning at the cone surface is assumed to produce an approximate half-cone of 15° included angle, from which the average flame zone Mach number may be calculated as in the previous section. The surface pressure in the disturbed region has been taken as twice the undisturbed cone surface pressure, and the remaining input parameters were chosen as in the previous section. The characteristic length of the system, L, was taken as five feet.

The results are shown in Figures 18 and 19. Once again, the lack of sensitivity of the heat transfer coefficient to the input parameters (η and T_w in this case) is demonstrated in Figure 18, where h is seen to fall within a relatively narrow band for the ranges

$$500^{\circ}R \leq T_w \leq 4000^{\circ}R$$
$$0.01 \leq \eta \leq 1.00$$

For computational purposes involving approximately similar trajectories the heat transfer coefficient may be selected from Figure 18.

The corresponding values of heat transfer rates to the vehicle wall are shown in Figure 19. The greater sensitivity of q_w to the input data may again be seen. However, the presented data may be used as an order-of-magnitude estimate of the wall heat transfer rates.

It should be noted in Figure 19 that for high values of T_w and low values of η at high altitude the heat transfer to the wall becomes negative. This corresponds to the case where $T_{ad} < T_w$ which is the case where the wall has an internal heat-generation mechanism. Clearly, in the present context this is not a physical solution.

In the utilization of heat transfer data the dimensionless Nusselt number is often used in the presentation of results. This parameter is defined as

$$Nu \equiv \frac{hL}{k}$$

where k is the thermal conductivity of the gas. In evaluating the thermal conductivity, the Eucken expression for polyatomic gases at low density was used[16]:

$$k = \left(\bar{c}_p + \frac{5}{4}\,\frac{R_o}{\mathcal{M}}\right)\mu$$

where the viscosity, μ, was computed from Equation (36). As may be seen in Figure 20, the Nusselt number varies from about 1×10^4 to 4×10^4 for the trajectory under consideration.

VI. CONCLUDING REMARKS

An approximate analysis of heat transfer to a flat plate in the presence of combustion has been formulated. The results generated by this analysis are in reasonable quantitative agreement with the results of a series of experiments conducted in a Mach 3.1 nozzle, using the pyrophoric fuel triethylaluminum. Although it was initially assumed that a constant value of equivalence ratio exists along the plate surface, it was found that the trend of the theoretical curves best correspond with the experimental trends when the analysis is modified to include the effect of variable $\eta(d\eta/dx > 0)$. In any event, it may be concluded on the basis of this comparison that the analysis will yield heat transfer rates and heat transfer coefficients which are in order-of-magnitude agreement with the experimental values, and are sufficiently accurate for most engineering design calculations.

It was found that the theoretical values of h and q_w are fairly insensitive to the local values of molecular weight and Prandtl number. In addition, the heat transfer coefficient was found to be only a weak function of the equivalence ratio, while q_w depends upon η to a much larger extent, through the dependence of the adiabatic wall temperature on the progress of the combustion process. Although both heat transfer parameters are strong functions of the local specific heat, this latter parameter varies over a relatively restricted range and may be estimated with sufficient accuracy by reference to the literature (e.g., Reference 15).

A relatively simple experimental technique for obtaining values of heat transfer coefficients and rates, and the theoretical analysis which suggests this technique were discussed. The experimental results serve as a basis for the above evaluation of the theoretical analysis developed in Section II.

Finally, estimates were made of h and q_w at the surface of a cone-shaped interceptor executing a coast trajectory in the altitude range 3000'-20,000'. It was assumed that an external burning-control force generation process is occurring at the cone surface, and that the vehicle is sufficiently large that local curvature effects may be ignored. It was found that for extensive ranges of equivalence ratio and wall temperature ($0.01 \leq \eta \leq 1.00$; $500^{\circ}R \leq T_w \leq 4000^{\circ}R$), the heat transfer coefficient varies only slightly. As a result, h may be estimated without precise knowledge of η and T_w. However, the wall heat transfer rate is a stronger function of these two parameters. Curves of Nusselt number for heat transfer were also presented. It is of interest to plot Nu as a function of the local Reynolds number in the manner suggested by Reference 17. Such a plot is shown in Figure 21 for several computed values of Nu and Re. Knudsen and Katz[17] point out that the expression which may be derived for a flat plate with constant wall temperature,

$$Nu = 0.0366\ (Re)^{4/5}\ (Pr)^{1/3} \qquad (39)$$

has also been found to agree with experimental results for heat transfer to a plate having variable surface temperature. Equation (39) is also shown in Figure 21. As may be seen, a satisfactory correlation is obtained when the constant in Equation (39) is changed to 0.0112. As a result, this empirical correlation may be used to obtain estimates for Nu for trajectories other than the one considered here.

VII. REFERENCES

1. Willmarth, W.W., "The Production of Aerodynamic Forces by Heat Addition on External Surfaces of Aircraft", The Rand Corp, RM-2078, December 30, 1957.

2. Luidens, R.W. and Flaherty, R.J., "Analysis and Evaluation of Supersonic Underwing Heat Addition", NASA Memo 3-17-59E, April 1959.

3. Chinitz, W., "Forces Induced by Combustion on a Flat Plate in Supersonic Flow", GASL Technical Report 434, April 1964 (Report Confidential-Title Unclass.)

4. Chinitz, W., and Spadaccini, L., "The Effects of Free-Stream Conditions on Force Generation by External Combustion on a Flat Plate in Mach 3.1 Flow", GASL Technical Report 472, October 1964, (Report Confidential-Title Unclass.)

5. Billig, F.S., "Supersonic Combustion of Storable Liquid Fuels in Mach 3.0 to 5.0 Air Streams", Tenth Symposium (International) on Combustion, August , 1964.

6. Dorsch, R.G., Serafini, J.S., and Fletcher, E.A., "Exploratory Investigation of Aerodynamic Effects of External Combustion of Aluminum Borohydride in Airstream Adjacent to Flat Plate in Mach 2.46 Tunnel", NACA Rept. RME57E16, July 29, 1957.

7. Grubman, D., Stroup, K.E., and Barber, K. F., "Applied Research Program-Aerospace Vehicle Interception Propulsion Program-Phase II", Marquardt Rept. S-346, October 25, 1963 (Report Confidential-Title Unclass.)

8. Kranz, P.C., and Pelkey, D.A., "Experimental Investigation of External Burning on an 8° Half-Angle Cone at Mach 5.0 and 6.1", Boeing Rept. D2-36037-1, July 1964.

9. Wu, J.M., Chapkis, R.L., and Mager, A., "Approximate Analysis of Thrust Vector Control by Fluid Injection", ARS Journal, 31 12, December 1961, pp. 1677-1685

10. Broadwell, J.E., "An Analysis of the Fluid Mechanics of Secondary Injection for Thrust Vector Control", AIAA Journal, 1, 5, May 1963, pp. 1067-1075.

11. Walker, R.E., and Shardor, M., "Influence of Injectant Properties for Fluid Injection Thrust Vector Control", J. Spacecraft and Rockets, 1, 4, July-August 1964, pp. 409-413.

12. Mayer, E., "Analysis of Convective Heat Transfer in Rocket Nozzles", ARS Journal, 31, 7, July 1961, pp. 911-917.

13. Rosner, D.E., "Effects of Diffusion and Chemical Reaction on Convective Heat Transfer", ARS Journal, 30, 1, January 1960, pp. 114-115.

14. Cresci, R.J., and Libby, P.A., "Some Heat Conduction Solutions Involved in Transient Heat Transfer Measurements", Polytechnic Institute of Brooklyn, WADC TN 57-236, ASTIA AD 130800, September 1957.

15. Ames Research Staff, "Equations, Tables and Charts for Compressible Flow", NACA Rept. 1135, 1963.

16. Powell, H.N. and Suciu, S.N., Editors, "Properties of Combustion Gases/System: C_nH_{2n}-Air; Volume I, Thermodynamic Properties", McGraw - Hill Book Co., Inc., New York, 1955.

17. Bird, R.B., Stewart, W.E , and Lightfoot, E.N., "Transport Phenomena", John Wiley and Sons, New York, 1960, p. 257.

18. Knudsen, J.G., and Katz, D.L., "Fluid Dynamics and Heat Transfer", McGraw - Hill Book Co., Inc., New York 1958; pp. 487-490.

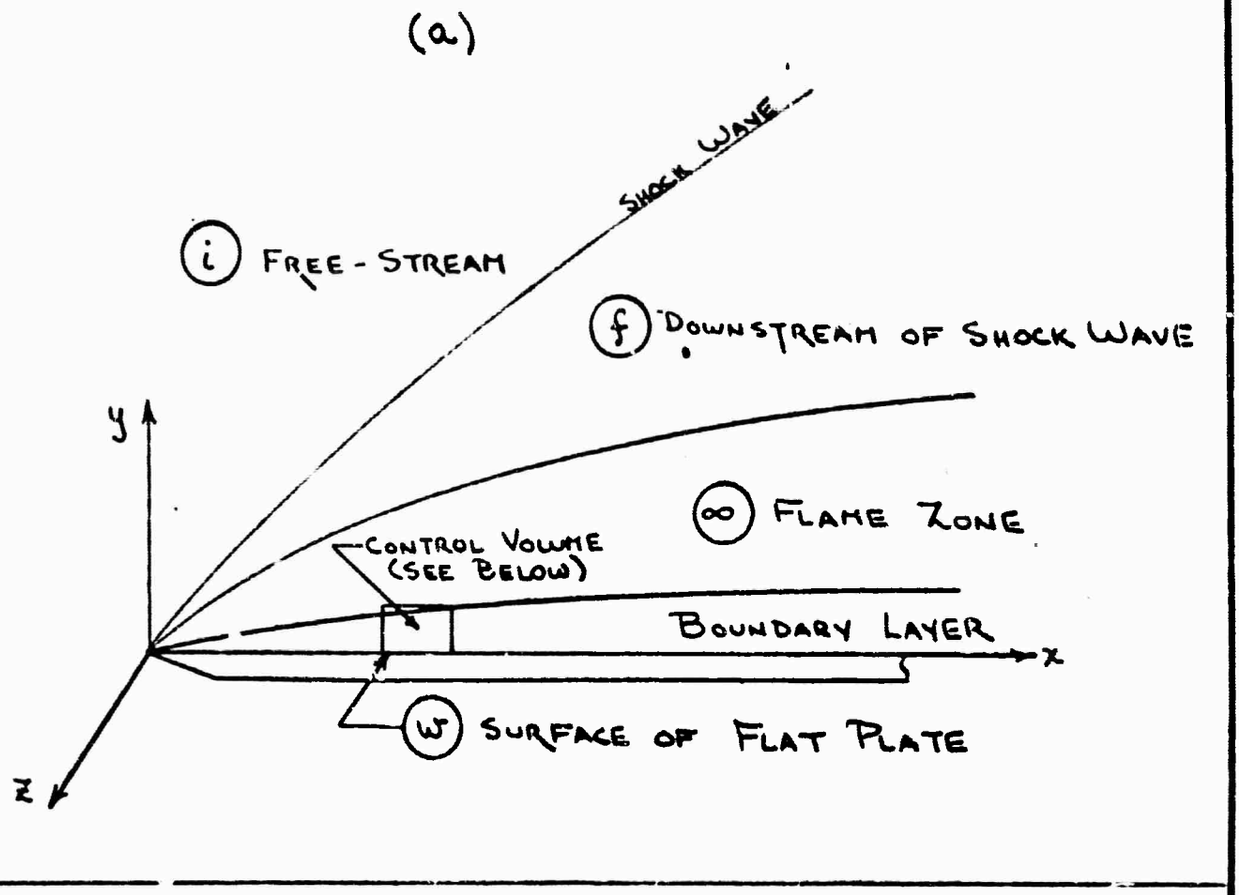

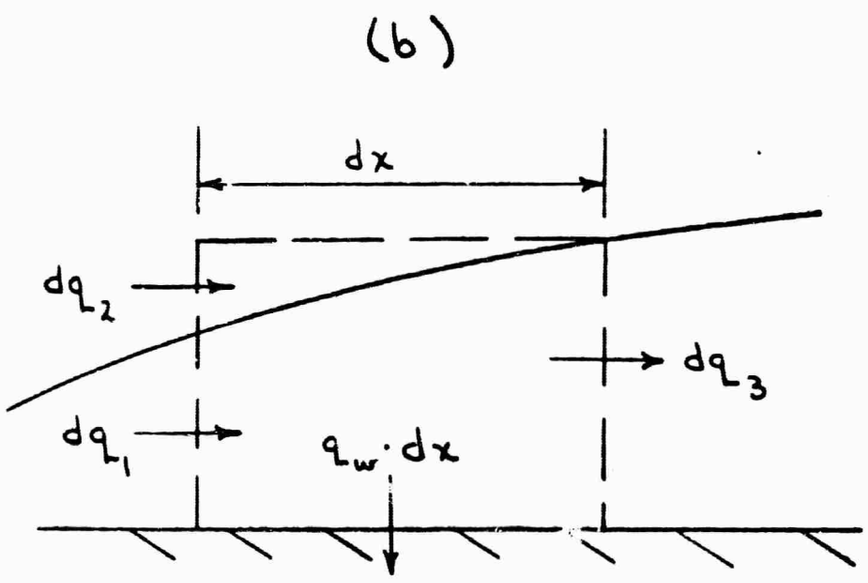

FIGURE 1. SCHEMATIC OF THE THEORETICAL MODEL

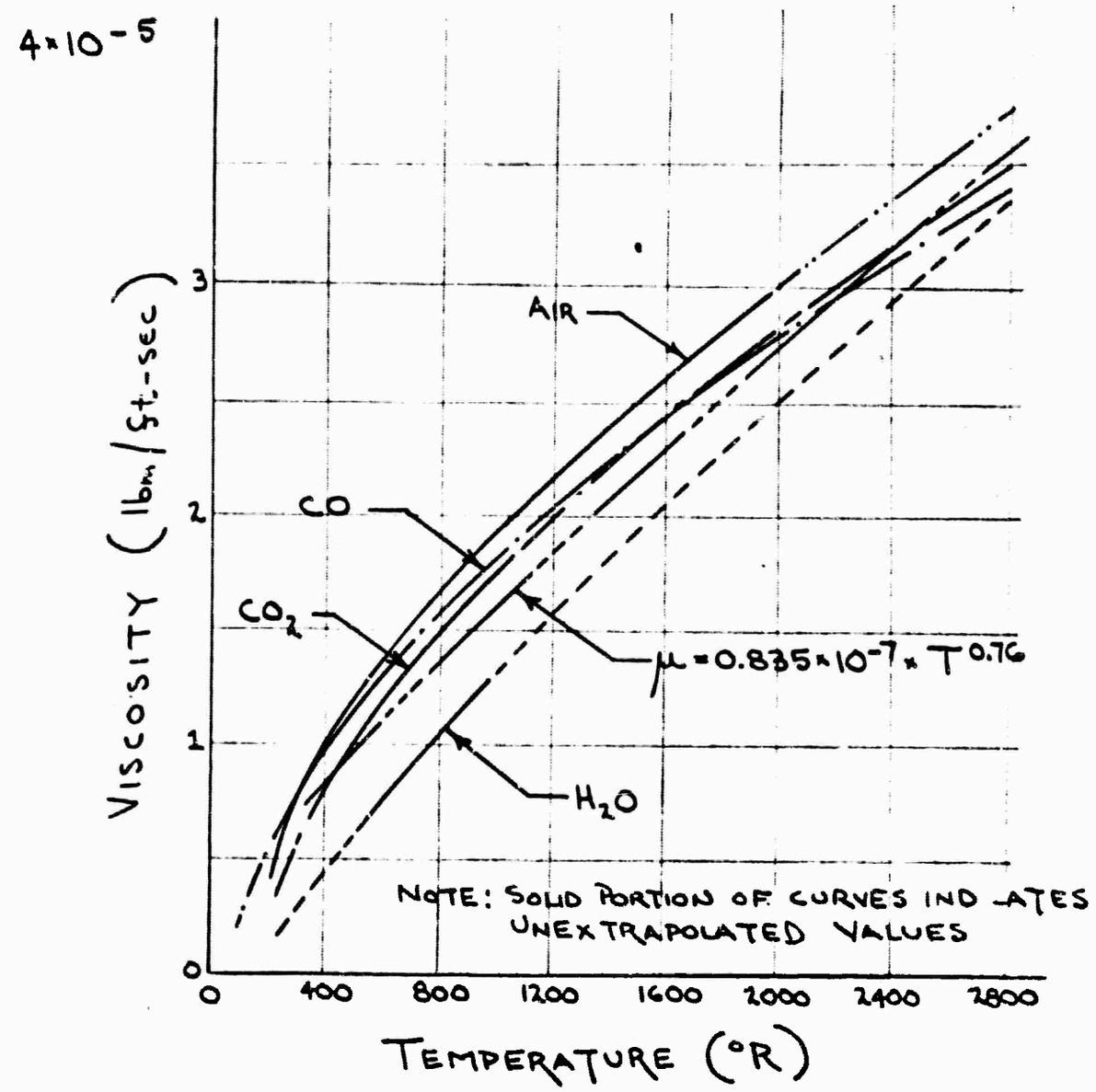

FIGURE 2. VISCOSITIES OF SEVERAL GASES

FIGURE 3. FLAT PLATE MODEL

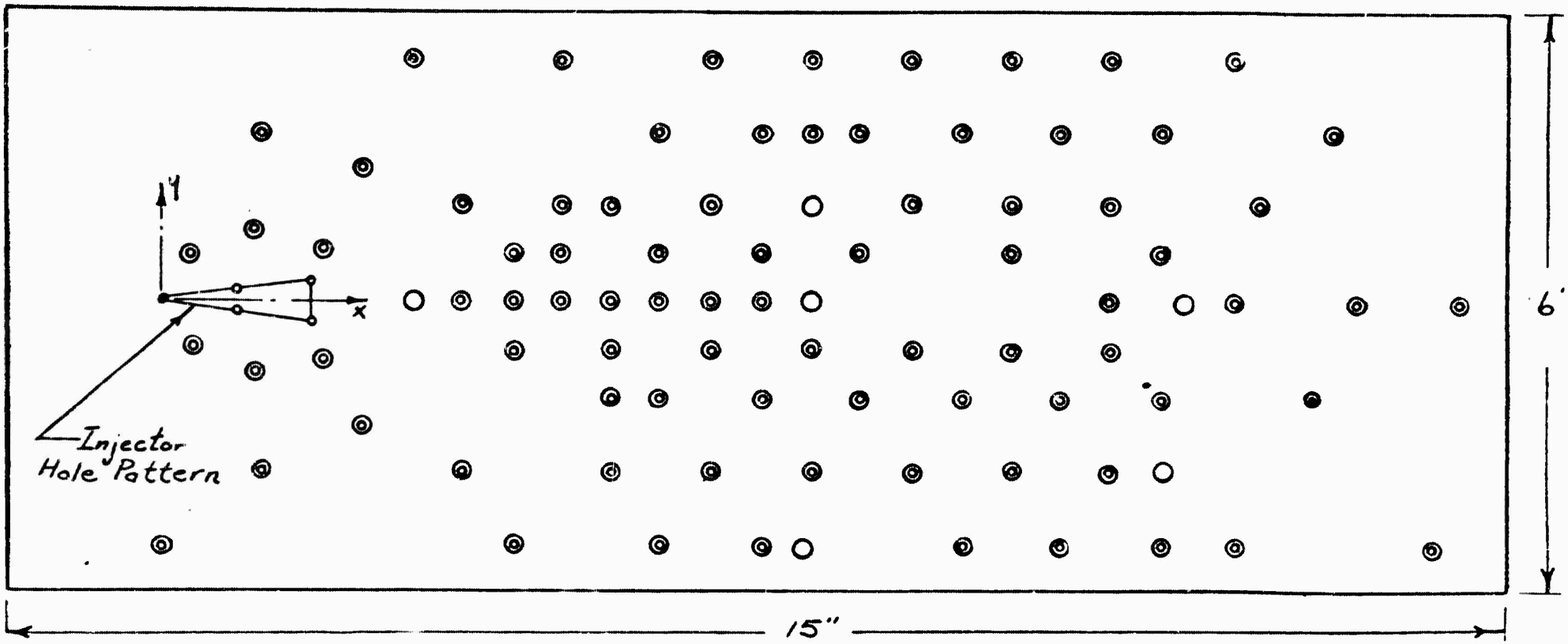

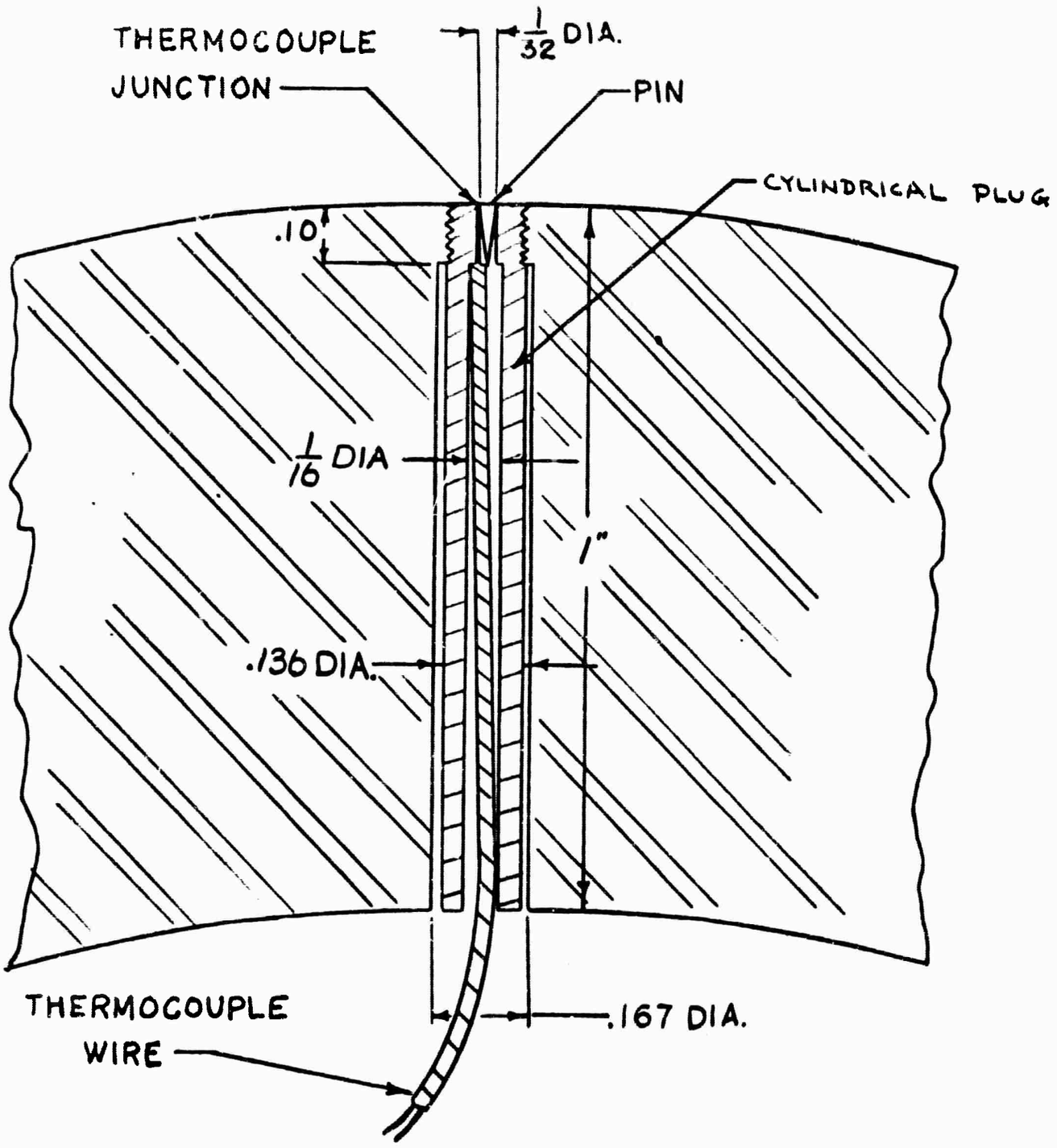

FIG. 4 TYPICAL THERMOCOUPLE INSTALLATION

FIGURE 3. FLAT PLATE MODEL

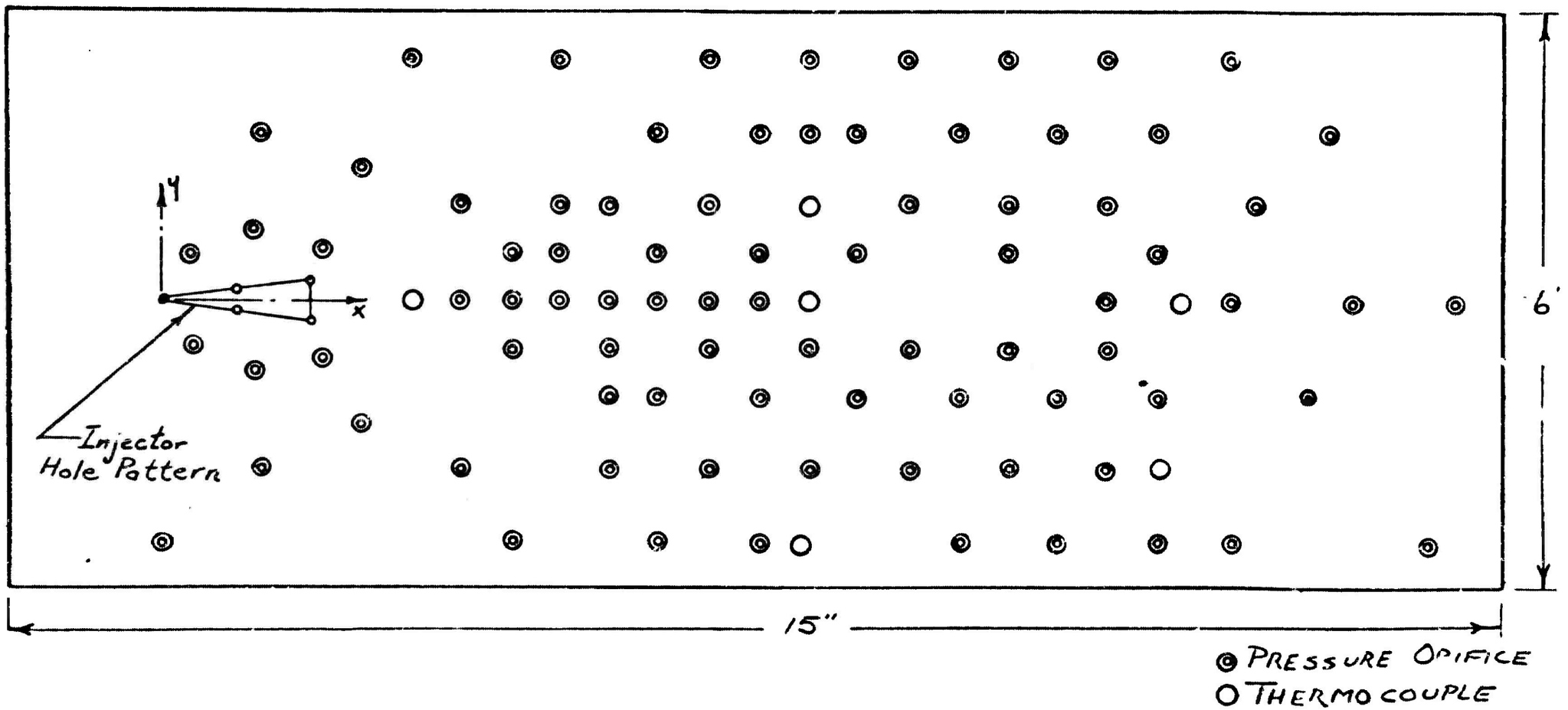

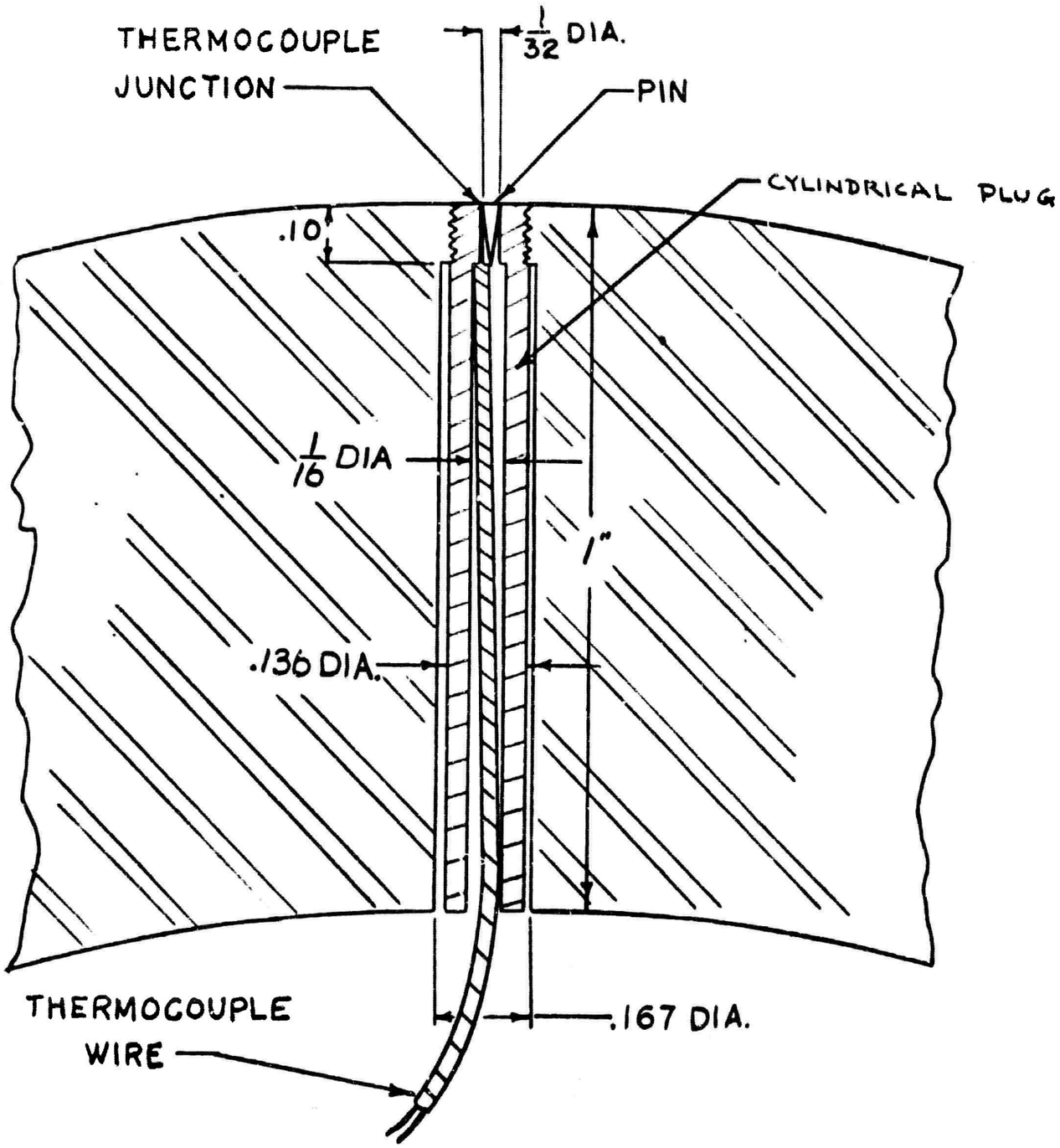

FIG. 4 TYPICAL THERMOCOUPLE INSTALLATION

FIGURE 5. MEASURED VALUES VS. TIME (LOW PRESSURE CASE)

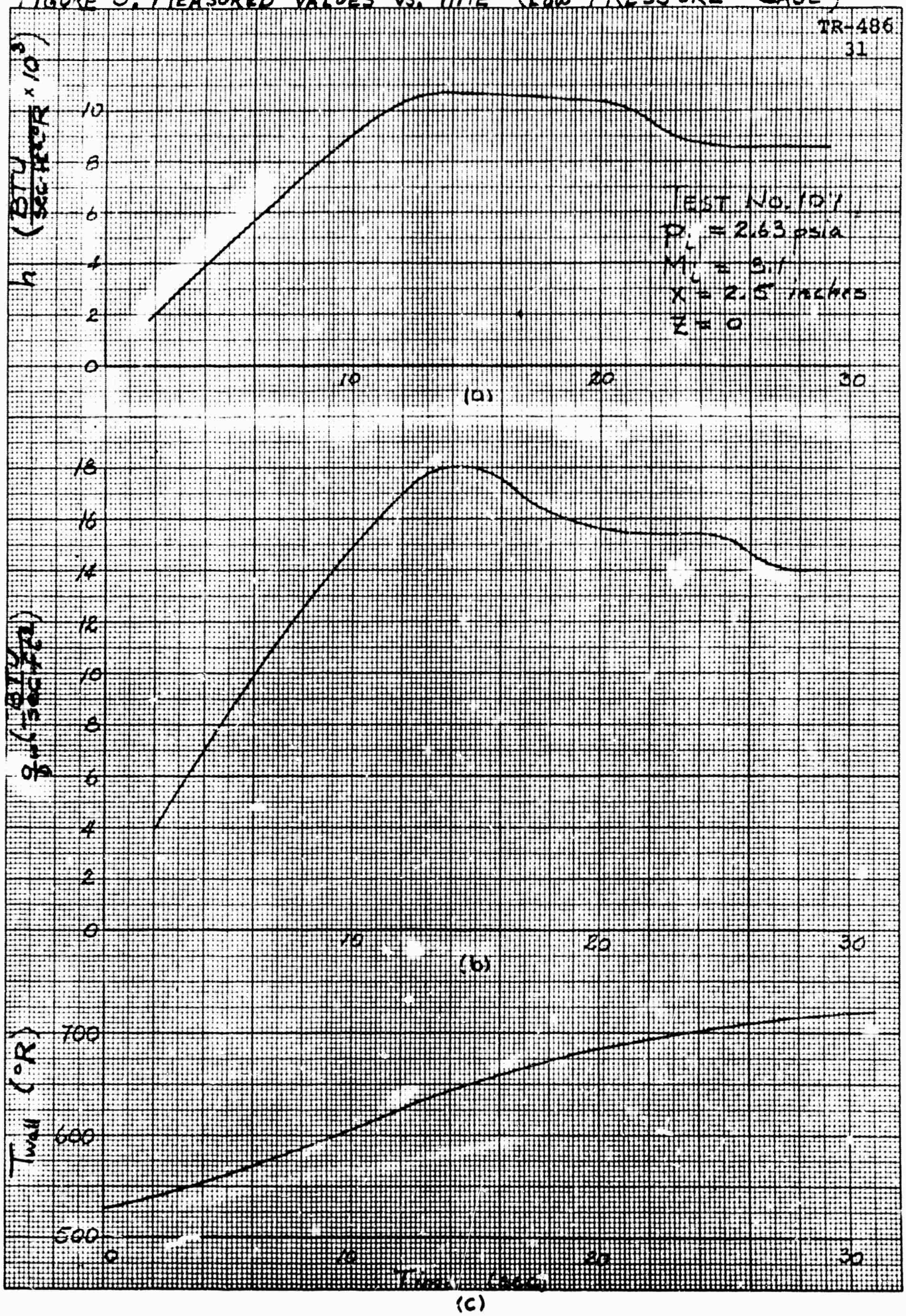

FIGURE 5 (CONTINUED)

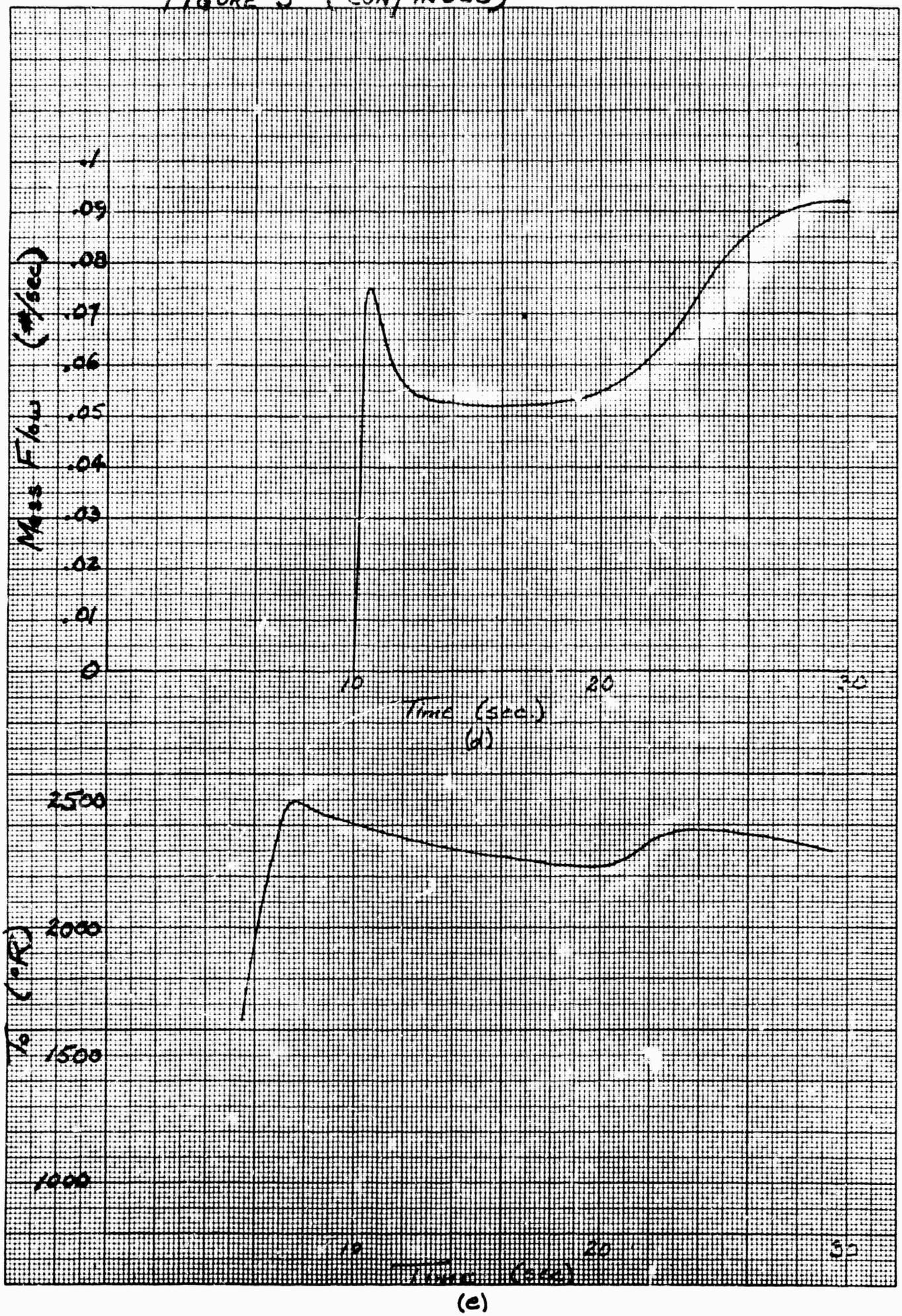

FIGURE 6. MEASURED VALUES VS TIME (INTERMEDIATE PRESSURE CASE)

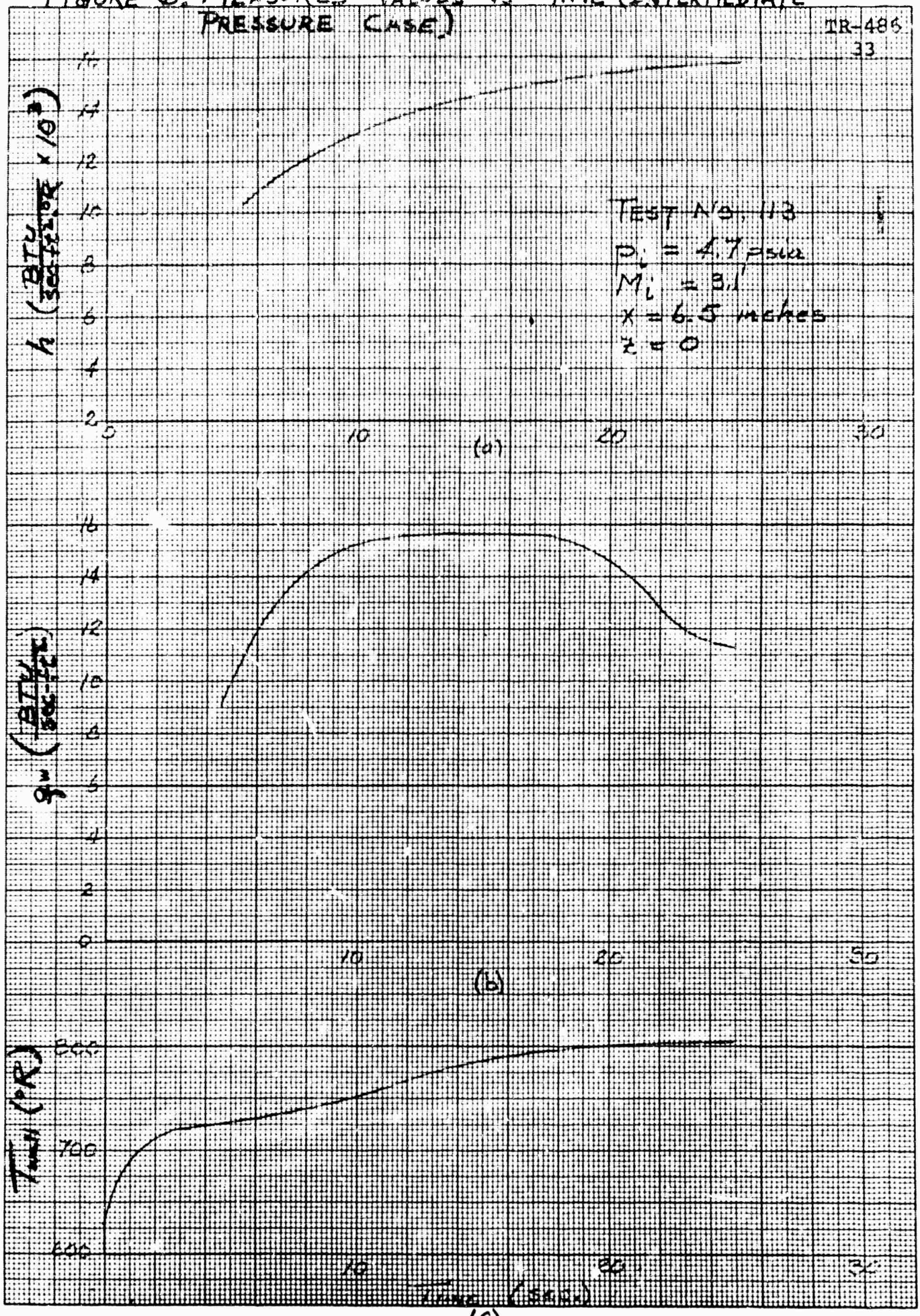

FIGURE 6 (CONTINUED)

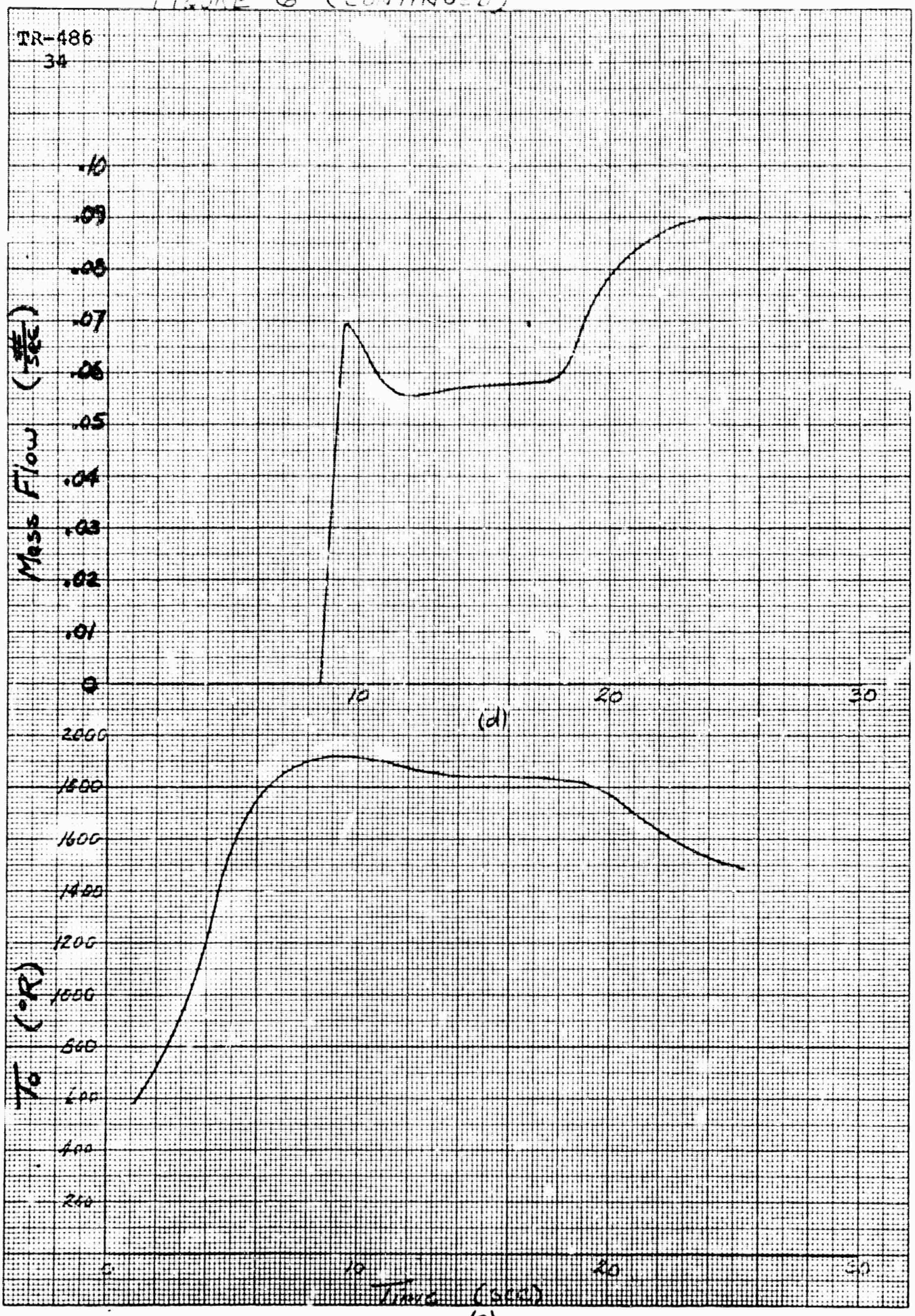

FIGURE 7. HEAT TRANSFER COEFFICIENT & HEAT TRANSFER RATE VS MASS FLOW RATE

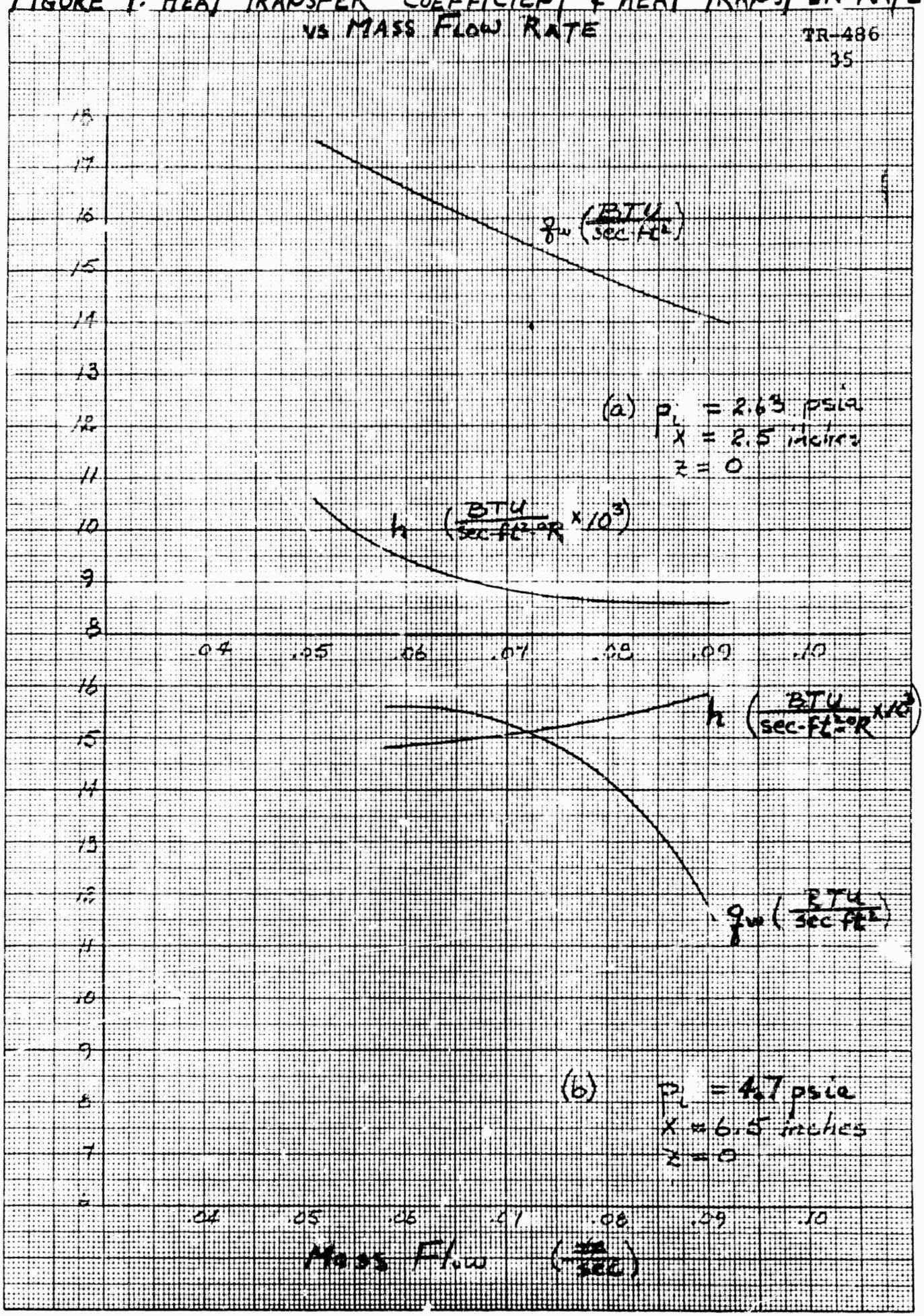

FIGURE 8. HEAT TRANSFER COEFFICIENT & HEAT TRANSFER RATE VS. AXIAL DISTANCE ALONG CENTERLINE

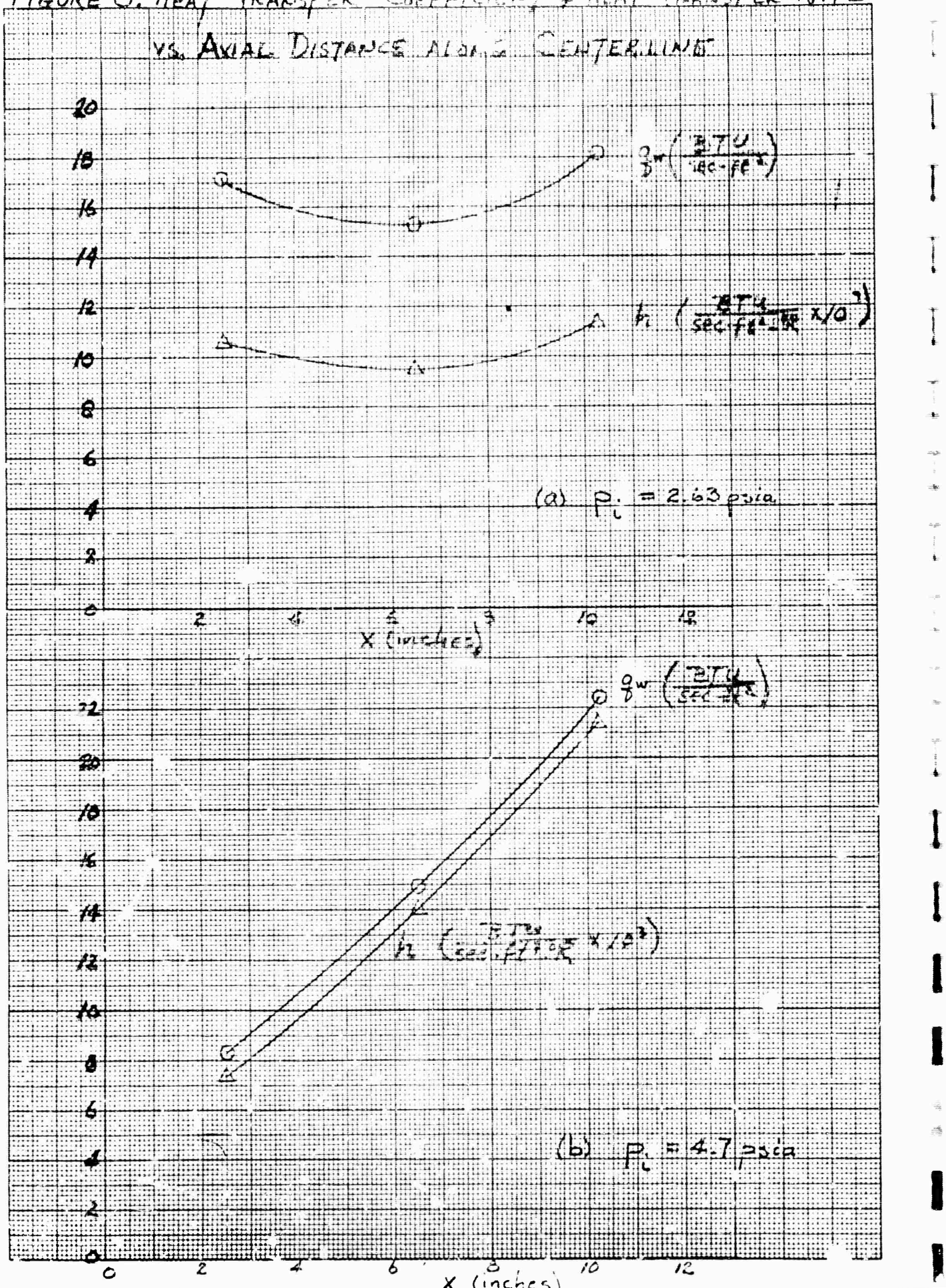

FIGURE 7. HEAT TRANSFER COEFFICIENT & HEAT TRANSFER RATE VS. DISTANCE FROM CENTERLINE FOR $X = 6.5$ INCHES

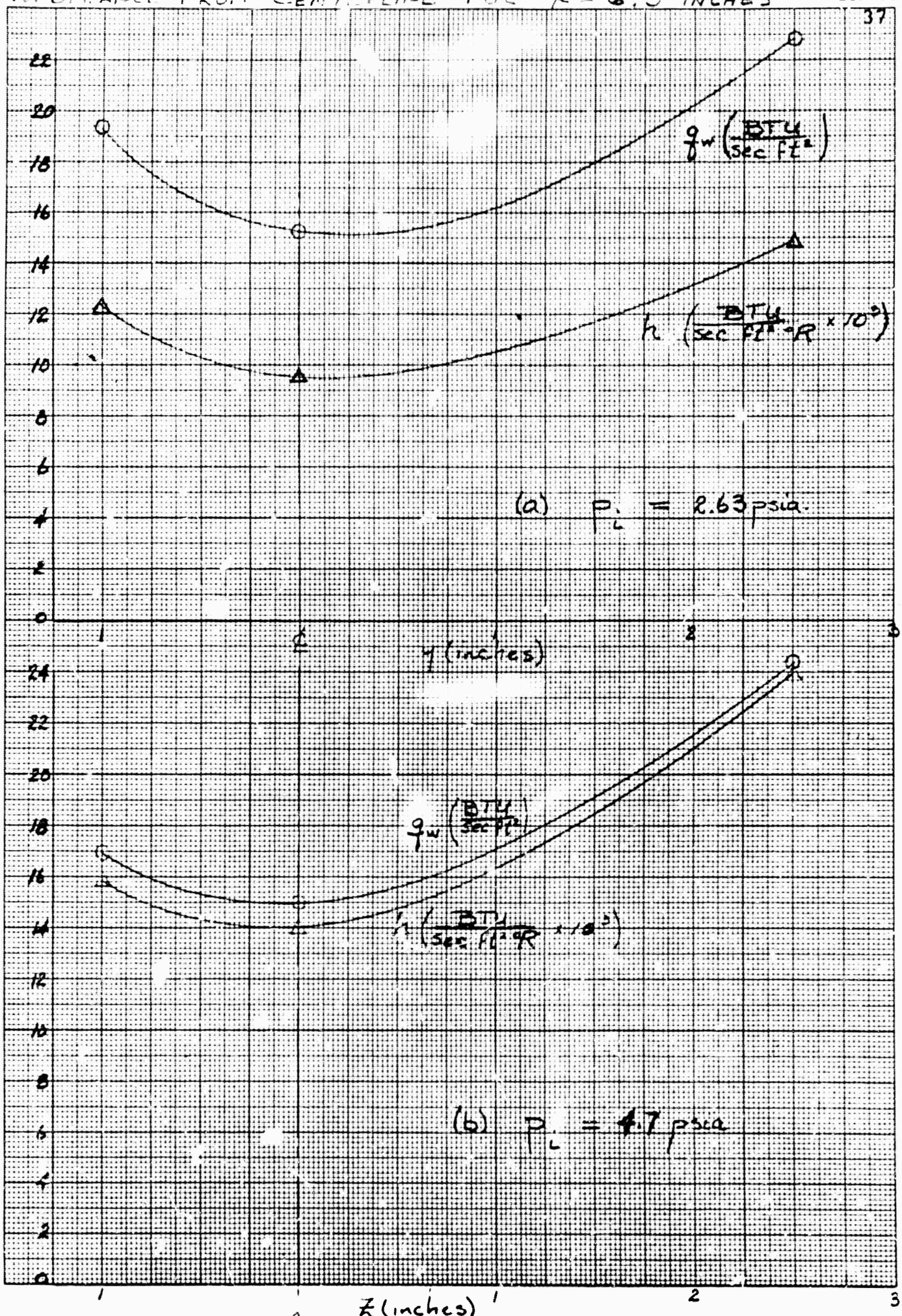

FIGURE 10. COMPARISON BETWEEN THEORETICAL [illegible] AND EXPERIMENTAL HEAT TRANSFER COEFFICIENTS (LOW PRESSURE CASE)

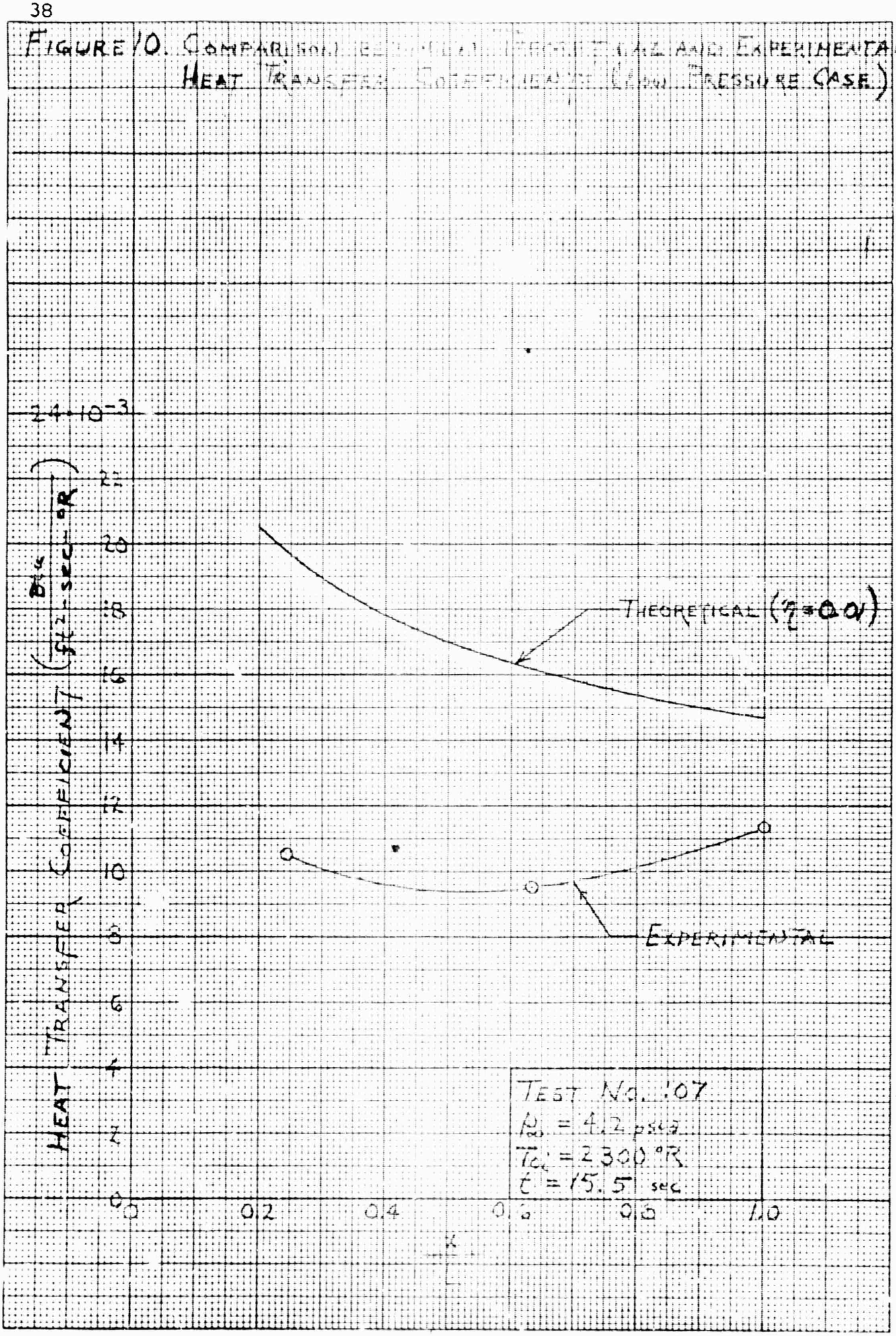

FIGURE 11. COMPARISON BETWEEN THEORETICAL AND EXPERIMENTAL HEAT TRANSFER RATES TO THE WALL (LOW PRESSURE CASE)

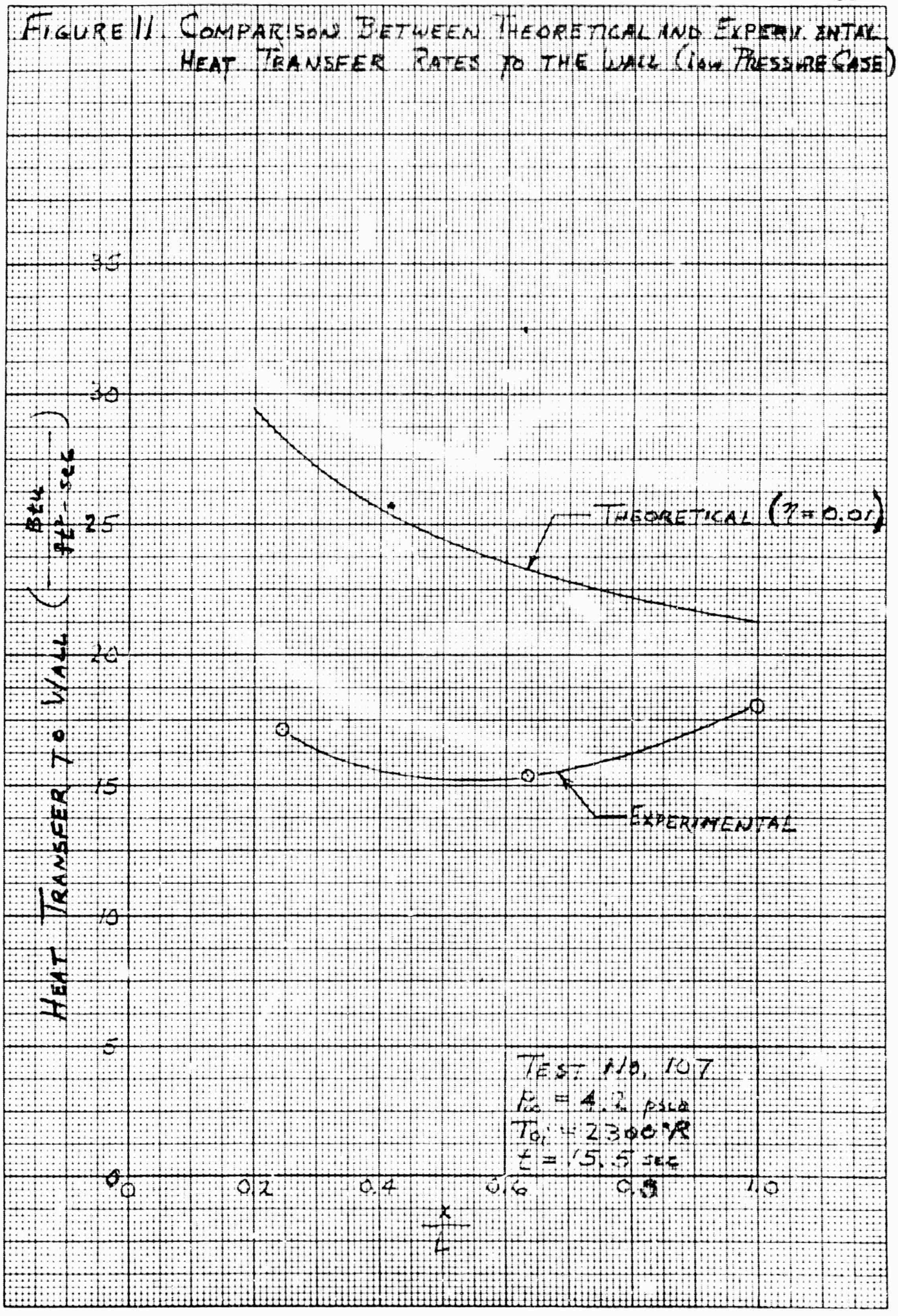

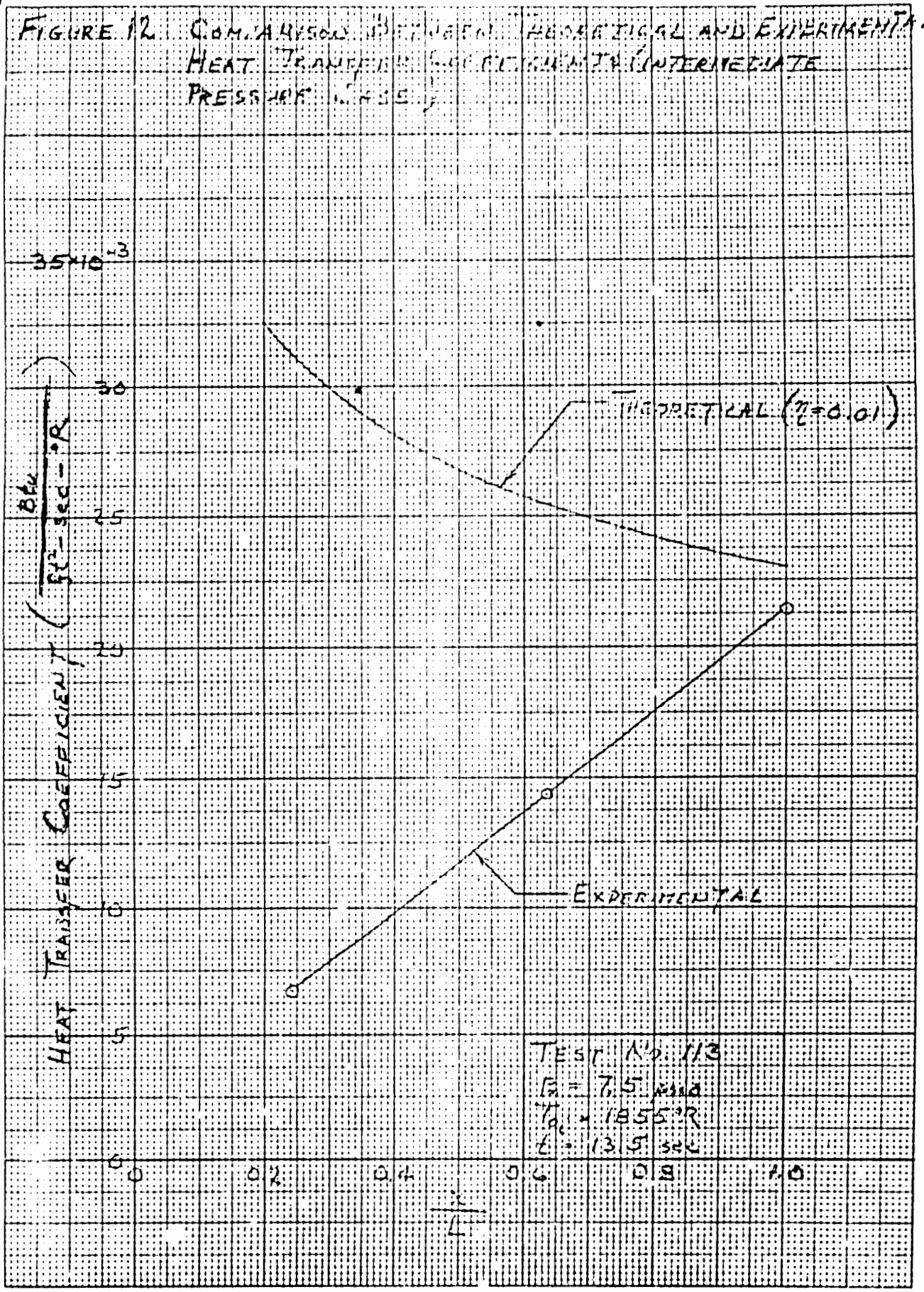

FIGURE 12. COMPARISON BETWEEN THEORETICAL AND EXPERIMENTAL HEAT TRANSFER COEFFICIENTS WITH INTERMEDIATE PRESSURE [illegible]

FIGURE 13. COMPARISON BETWEEN THEORETICAL AND EXPERIMENTAL HEAT TRANSFER RATES TO THE WALL (INTERMEDIATE PRESSURE CASE)

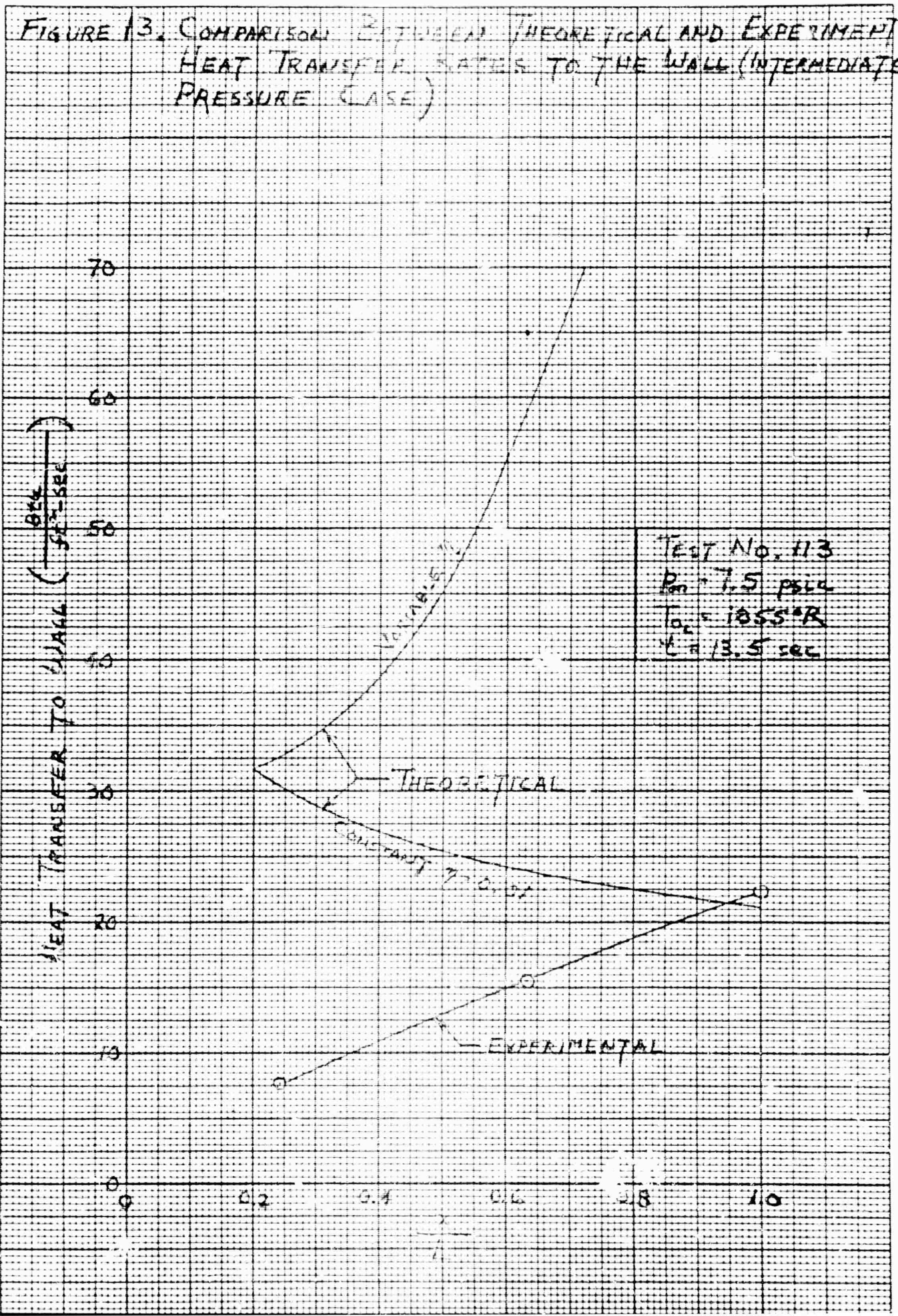

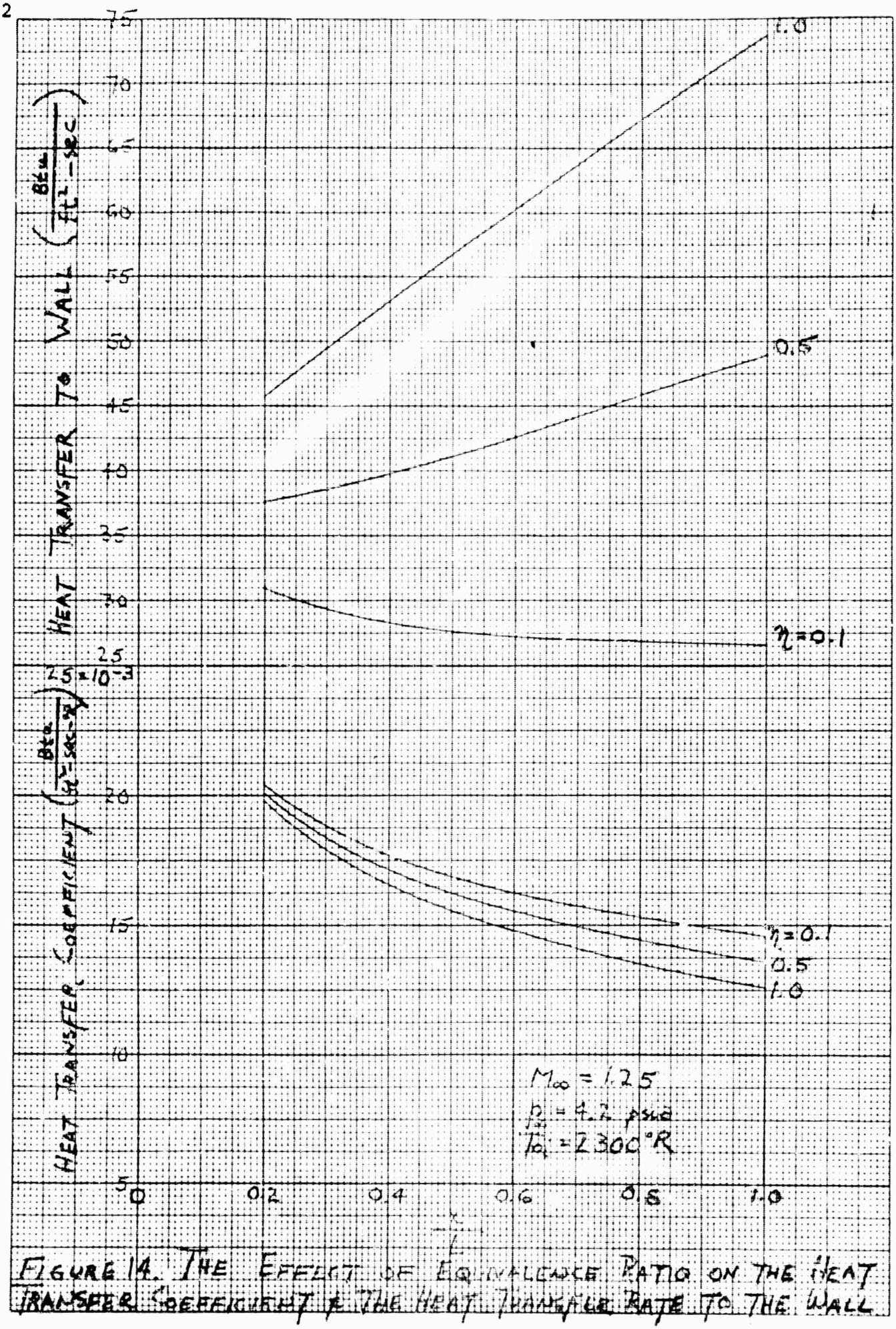

FIGURE 14. THE EFFECT OF EQUIVALENCE RATIO ON THE HEAT TRANSFER COEFFICIENT & THE HEAT TRANSFER RATE TO THE WALL

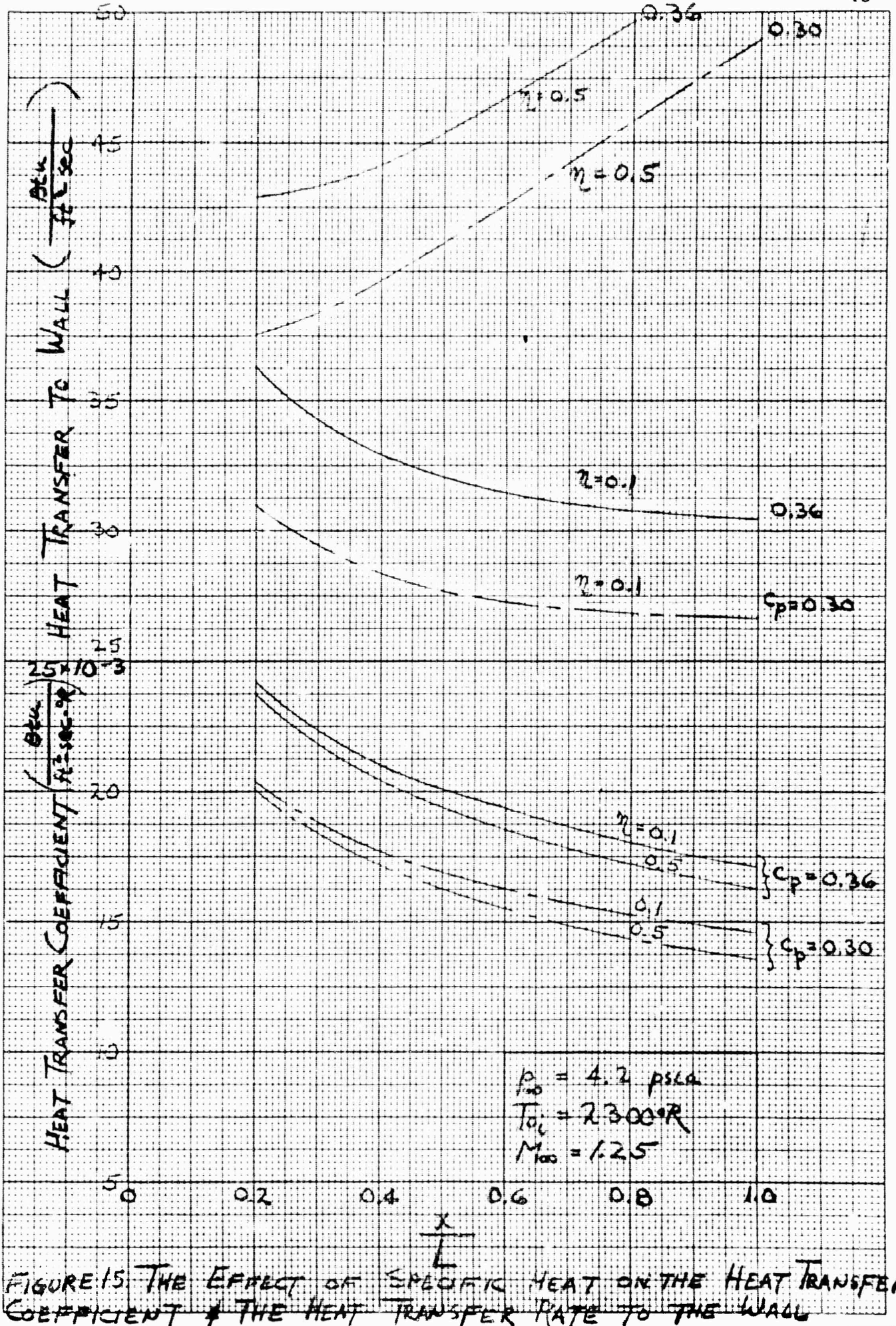

FIGURE 15. THE EFFECT OF SPECIFIC HEAT ON THE HEAT TRANSFER COEFFICIENT & THE HEAT TRANSFER RATE TO THE WALL

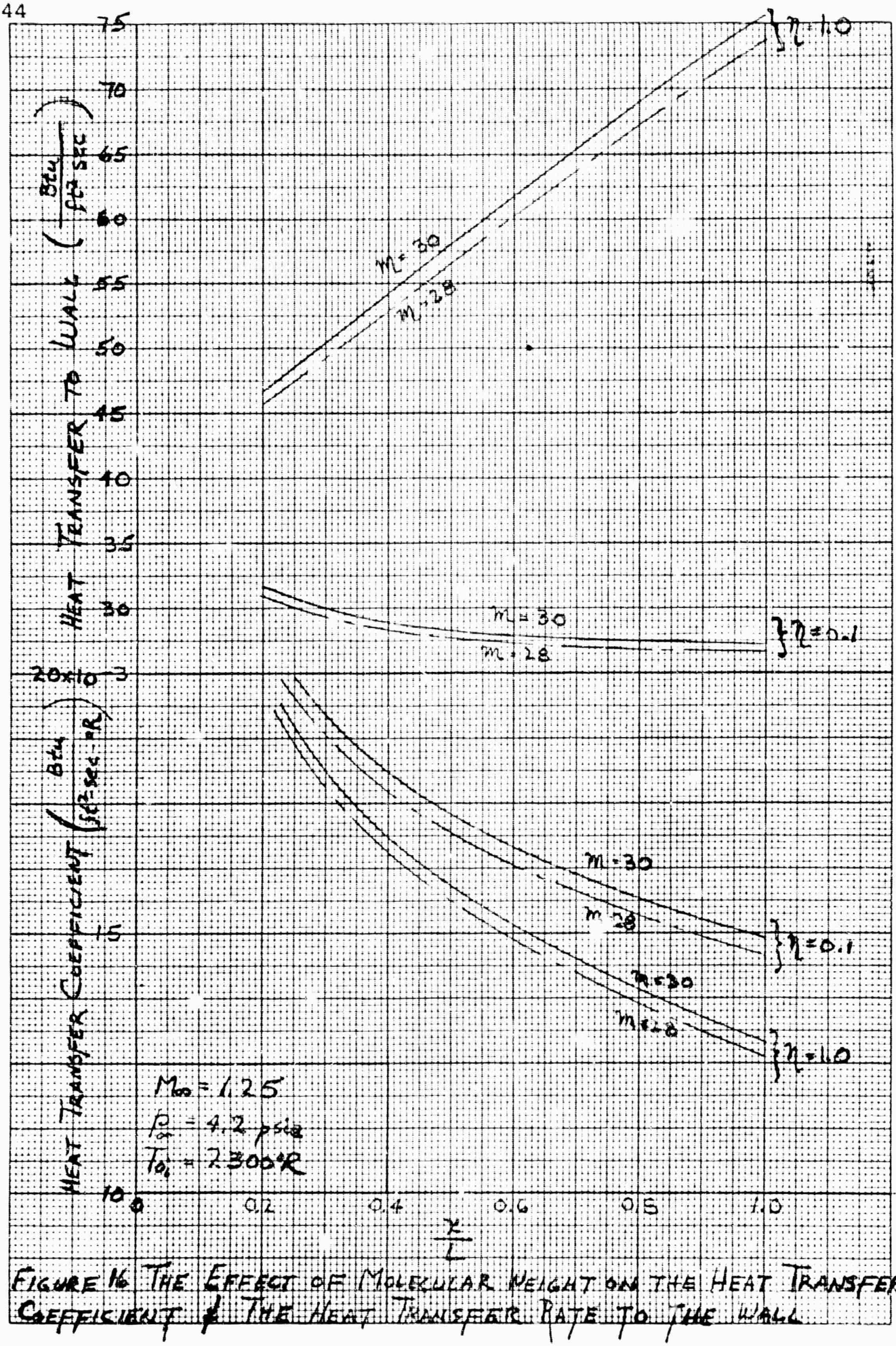

FIGURE 16 THE EFFECT OF MOLECULAR WEIGHT ON THE HEAT TRANSFER COEFFICIENT & THE HEAT TRANSFER RATE TO THE WALL

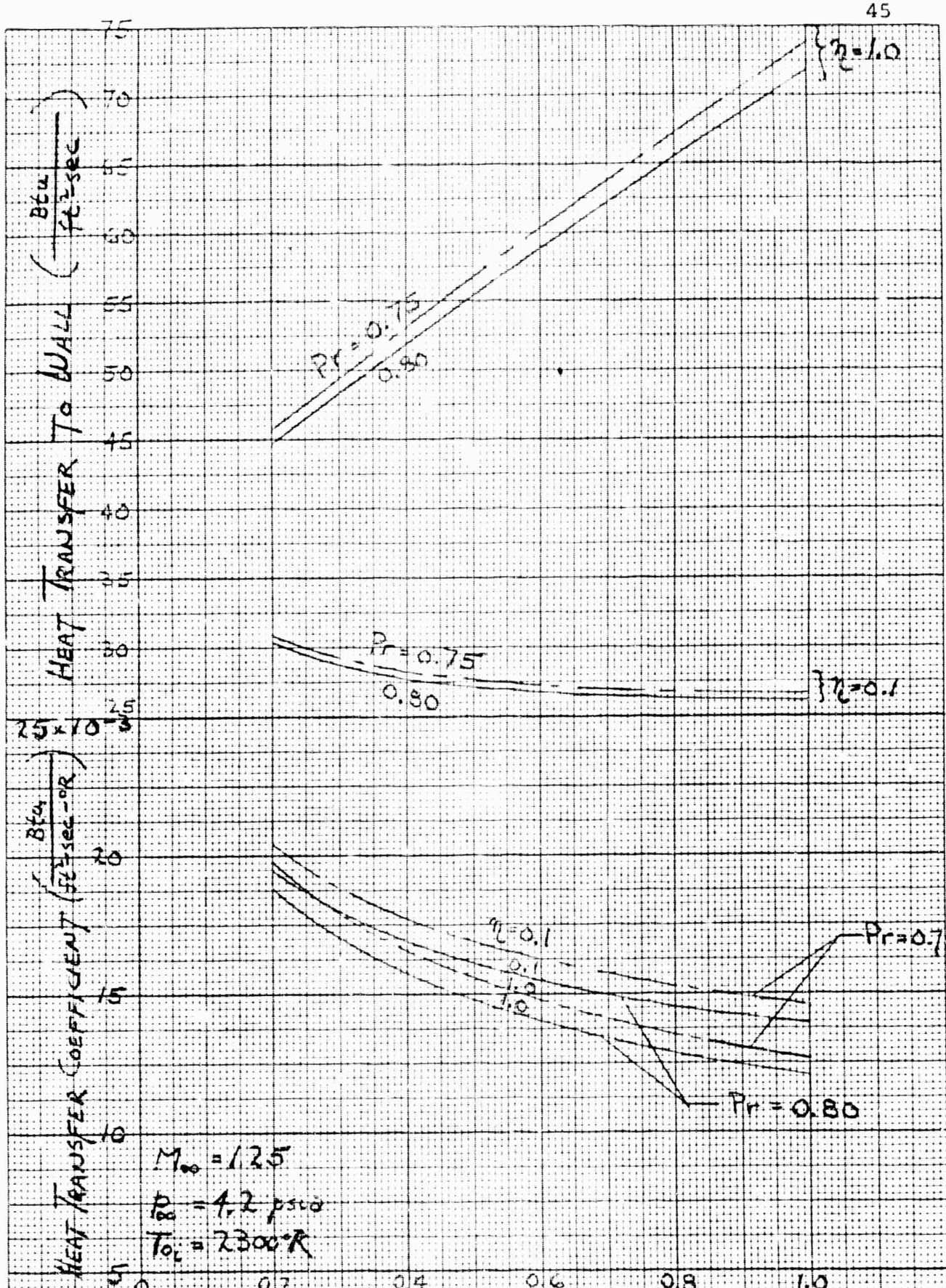

FIGURE 17. THE EFFECT OF PRANDTL NUMBER ON THE HEAT TRANSFER COEFFICIENT & THE HEAT TRANSFER RATE TO THE WALL

FIGURE 18 HEAT TRANSFER COEFFICIENTS ON THE SURFACE OF THE FLIGHT VEHICLE

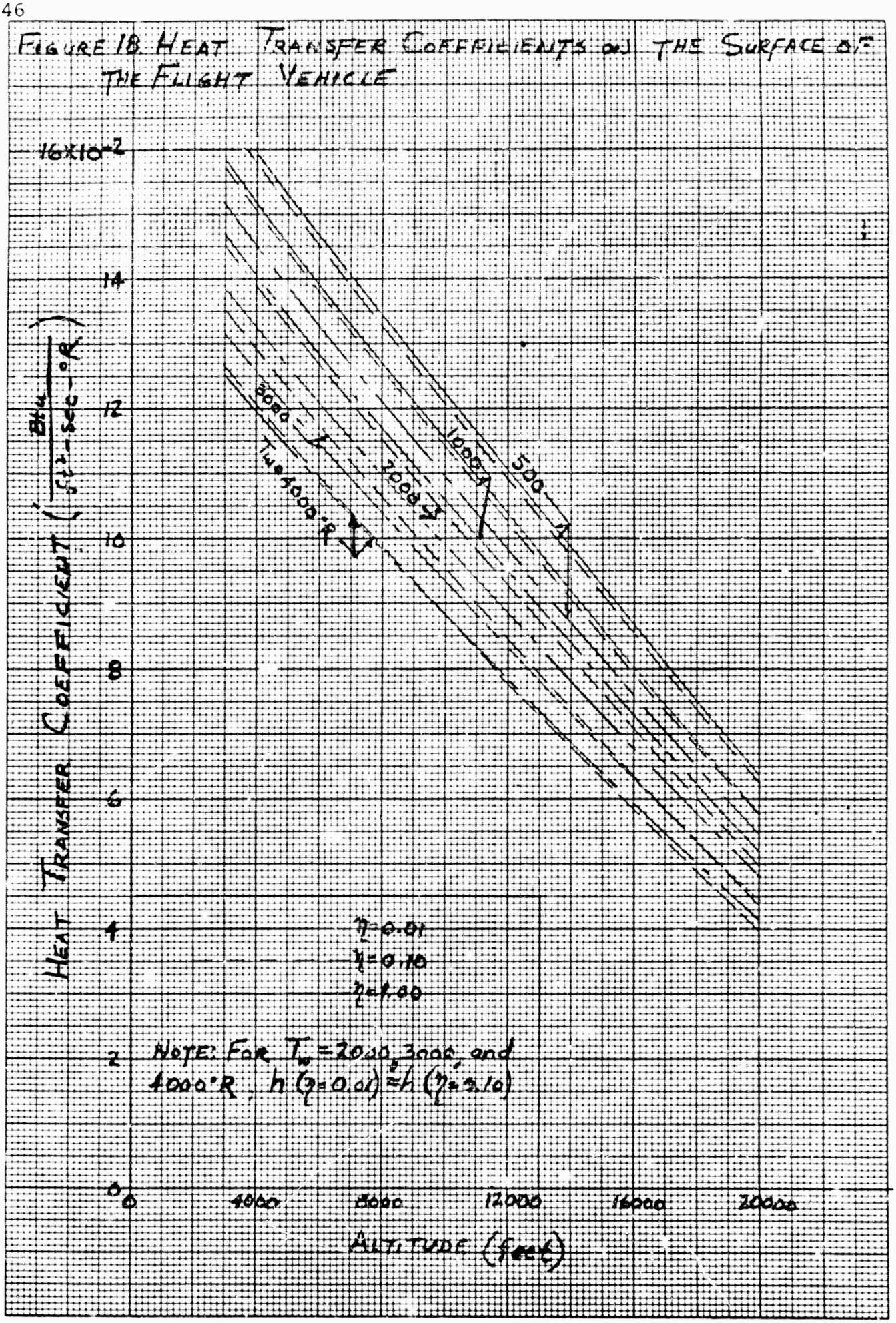

BLANK PAGE

FIGURE 19. HEAT TRANSFER RATES TO THE SURFACE OF THE FLIGHT VEHICLE

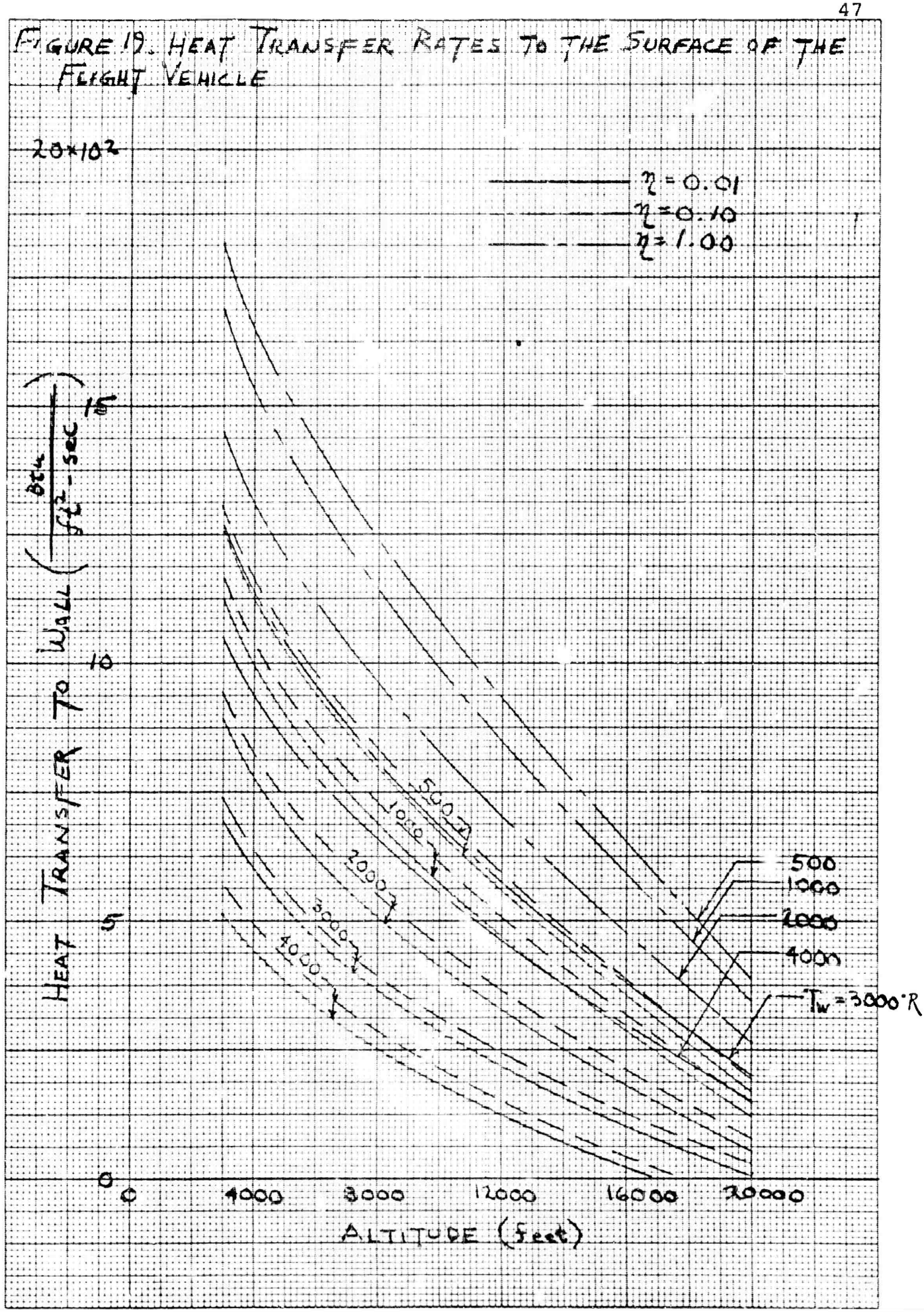

FIGURE 20 NUSSELT NUMBERS FOR HEAT TRANSFER ON THE SURFACE OF THE FLIGHT VEHICLE

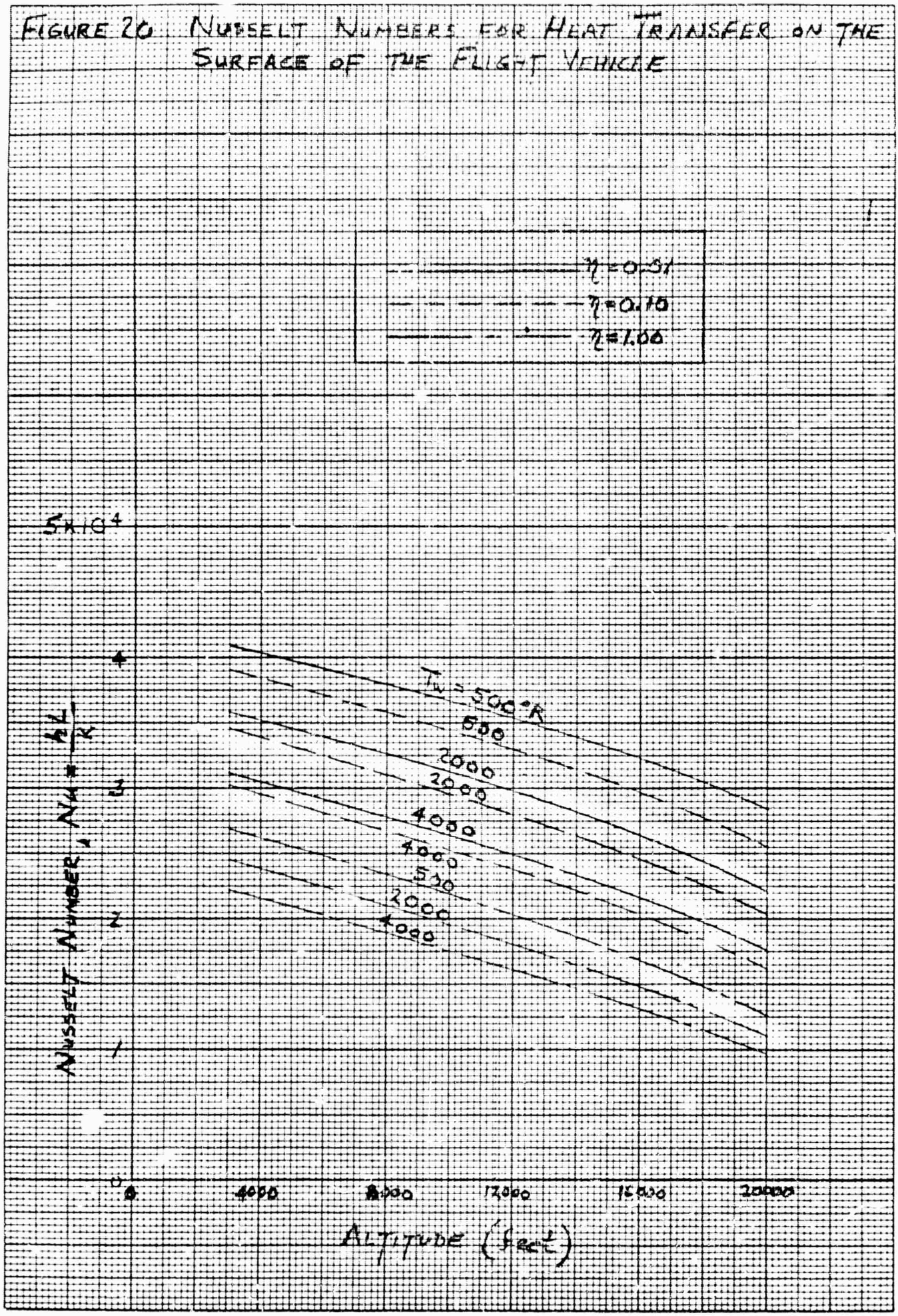

FIGURE 21. CORRELATION BETWEEN NUSSELT & REYNOLDS NUMBERS